Seasonal variability and sources of *in situ* brGDGT production in a permanently stratified African crater lake

Loes van Bree[a], Francien Peterse[a*], Allix Baxter[a], Wannes De Crop[b], Sigrid van Grinsven[c], Laura Villanueva[c], Dirk Verschuren[b], Jaap Sinninghe Damsté[a,c]

[a] Utrecht University, Faculty of Geosciences, Department of Earth Sciences, Princetonlaan 8A, 3584 CD Utrecht, The Netherlands.
[b] Ghent University, Limnology Unit, K.L. Ledeganckstraat 35, B-9000 Gent, Belgium.
[c] NIOZ Royal Netherlands Institute for Sea Research, Department of Marine Microbiology and Biogeochemistry, and Utrecht University, PO Box 59, 1790 AB Den Burg, The Netherlands.

*Corresponding author. Utrecht University, Faculty of Geosciences, Department of Earth Sciences, Princetonlaan 8A, 3584 CD Utrecht, The Netherlands. F.Peterse@uu.nl.

Keywords:

brGDGTs, East Africa, lake, *in situ* production, 16S rRNA gene amplicon sequencing

Highlights:

- BrGDGTs in the tropical African lake Chala are produced *in situ*
- Acidobacteria are not the dominant source of aquatic brGDGTs
- Stratification and mixing drive aquatic brGDGT production and their signature

Abstract

Lake sediments are important archives of continental climate history, and their lipid biomarker content can be exploited to reconstruct paleoenvironmental conditions. Branched glycerol dialkyl glycerol tetraethers (brGDGTs) are bacterial membrane lipids widely used in paleoclimate studies to reconstruct past temperature. However, major gaps still exist in our understanding of the environmental controls on *in situ* (i.e., aquatic) production in lake systems. In Lake Chala, a permanently stratified tropical crater lake in East Africa, we determined the concentrations and fractional abundances of individual brGDGTs along depth profiles of suspended particulate matter collected monthly from September 2013 to January 2015, and in settling particles collected monthly at 35 m water depth from August 2010 to January 2015, and compared these brGDGT distributions with those in surficial lake-bottom sediments and catchment soils. We find that brGDGTs are primarily produced within the water column, and that their concentrations and distributions vary greatly with depth and over time. Comparison with concentration-depth profiles of the monthly distribution and abundance of bacterial taxa, based on 16S rRNA gene amplicon sequencing and quantification, indicates that Acidobacteria are likely not the main producers of brGDGTs in Lake Chala. Shallowing of the oxic-anoxic boundary during seasonal episodes of strong water-column stratification promoted production of specific brGDGTs in the anoxic zone. BrGDGT distributions in the water column do not consistently relate with temperature, pH, or dissolved-oxygen concentration, but do respond to transitions between episodes of strong stratification and deep (but partial) lake mixing, as does the aquatic bacterial community. Hence, the general link between brGDGT distributions and temperature in brGDGT-based paleothermometry is more likely driven by a change in bacterial community composition than by membrane adaptation of specific members of the bacterial community to changing environmental conditions. Although temperature is not the principal driver of distributional changes in aquatic brGDGTs in this system, at least not during the 17-month study period, abundance-weighted and time-integrated averages of brGDGT fractional abundance in the 53-month time series of settling particles reveal systematic variability over longer time scales that indirectly relates to temperature. Thus, although we do not as yet fully understand the drivers of modern-day brGDGT fluxes and distributions in Lake Chala, our data do support the application of brGDGT paleothermometry to time-integrated archives such as sediments.

1. Introduction

Lake sediments are important archives of continental climate history, especially in (sub-) tropical regions where other long-term, high-resolution natural archives such as ice cores are lacking. Lipid biomarkers preserved in those sediments can be used to examine present and past environmental conditions, and often provide more specific information on those conditions than bulk geochemical proxies (see Castañeda and Schouten, 2011 for a review). For example, plant waxes stored in lake sediments are used to reconstruct past vegetation and hydroclimate dynamics (e.g., Freeman and Pancost, 2013; Diefendorf and Freimuth, 2017), while the presence and distribution of (iso-)loliolide, long-chain *n*-alk-1-enes or 1,15 *n*-alkyl diols can be linked to shifts in algal community composition and/or primary productivity (e.g., Volkman et al., 1998; Castañeda and Schouten, 2011; van Bree et al., 2018).

Temperature is probably the most important climate parameter to be reconstructed quantitatively from lacustrine settings. Although temperature variation in the tropics is relatively modest, even on glacial-interglacial timescales (2-4 °C at sea level; e.g. Loomis et al., 2017; Chevalier et al., 2020), this has major impact on tropical continental rainfall through its control on sea-surface evaporation and monsoon dynamics between the ocean and adjacent continents. Therefore, no rainfall or moisture-balance reconstruction from the tropics can be properly interpreted without knowing local/regional temperature history as reference frame. However, despite more than a decade of substantial effort, generating long and continuous quantitative temperature reconstructions from tropical regions remains challenging.

One promising proxy for continental paleothermometry is based on a suite of membrane lipids supposedly derived from bacteria, namely the branched glycerol dialkyl glycerol tetraethers (brGDGTs; Sinninghe Damsté et al., 2000). These consist of tetra- (I), penta- (II) or hexamethylated (III) components, with none (suffix a), one (b) or two (c) cyclopentyl moieties, and with methyl groups on the 5th (5-methyl) or 6th (6-methyl; indicated with a prime notation) carbon position of their alkyl chain (Fig. 1; Sinninghe Damsté et al., 2000; Weijers et al., 2006, De Jonge et al., 2013). The distribution of brGDGTs in modern surface soils and peats shows empirical relationships with mean annual air temperature (MAAT) and the pH of the soil or peat in which they are produced (Weijers et al., 2007b; De Jonge et al., 2014a; Naafs et al., 2017a,b). Although the bacteria that produce brGDGTs are still largely unknown (Sinninghe Damsté et al., 2018), this relationship has been commonly used as proxy for continental air temperature in paleoclimate reconstructions. For example, analysis of brGDGTs in loess soils, peats and marine sediments has produced

paleotemperature records across a wide range of geological ages (e.g., Weijers et al., 2007a; Peterse et al., 2011; Naafs et al., 2017a; Zheng et al., 2017).

The application of this temperature proxy on lake-sediment records was initially based on the premise that all sedimentary brGDGTs are derived from catchment soils and washed into the lake by erosion. However, when brGDGT distributions in lake sediments were found to differ substantially from those in soils surrounding the lake, it became clear that there must also be an *in situ* source of brGDGTs contributing to the lake sediments (e.g., Tierney and Russell, 2009; Tierney et al., 2009; Sinninghe Damsté et al., 2009; Loomis et al., 2011; Schouten et al., 2013; Buckles et al., 2014; Colcord et al., 2015; Li et al., 2016). In addition, brGDGT isomers of type IIIa with methyl branches at the 5th position on the one end and at the 6th position on the other end (IIIa″) have so far been detected exclusively in lakes and not in soils, providing further evidence for their *in situ* production (Weber et al., 2015, 2018). Furthermore, lacustrine brGDGTs are significantly more ^{13}C-depleted than those in nearby soils, implying that at least some of their sources are distinct (Weber et al., 2015; 2018; Colcord et al., 2017).

Water-column studies show that brGDGT concentrations generally increase below the oxycline, suggesting that they are mainly produced in the anoxic portion of the hypolimnion (Sinninghe Damsté et al., 2009; Bechtel et al., 2010; Blaga et al., 2011; Woltering et al., 2012; Buckles et al., 2014; Loomis et al., 2014b; Miller et al., 2018). Further, brGDGT production often varies seasonally (Sinninghe Damsté et al., 2009; Woltering et al., 2012; Buckles et al., 2014), which may introduce a temperature bias towards the season(s) with high brGDGT production (Loomis et al., 2014b; Miller et al., 2018). The contribution of aquatic brGDGTs, especially that of IIIa, generally results in a substantial underestimation of present-day temperature when the transfer function based on soil brGDGTs is used (Tierney et al., 2010), which has stimulated the development of temperature calibrations based on lake sediments (Tierney et al., 2010; Pearson et al., 2011; Sun et al., 2011; Loomis et al., 2012; Russell et al., 2018). As in soils, the amount and distribution of brGDGTs in lake sediments seems to be influenced mostly by temperature and lake-water pH (Tierney et al., 2010; Sun et al., 2011; Loomis et al., 2014a), although a wide range of other factors, such as oxygen availability (e.g., Tierney et al., 2012; Loomis et al., 2014a; Weber et al., 2018), light (Loomis et al., 2014b), mixing regime (Loomis et al., 2014b), nutrients (Tierney et al., 2010; Loomis et al., 2014a), alkalinity (Schoon et al., 2013), redox state (Weber et al., 2018) and conductivity (Tierney et al., 2010), have also been suggested to influence the *in situ* production of brGDGTs in lakes.

Temperature calibrations based on brGDGTs in soils and peats have substantially improved following the identification and chromatographic separation of 5-methyl and 6-methyl brGDGT isomers (De Jonge et al., 2014a; Naafs et al., 2017a, 2017b; Dearing Crampton-Flood et al., 2020). Initial scanning of surficial bottom sediments from East African lakes revealed that especially 6-methyl brGDGTs behave differently in lakes compared to soils, suggesting that they are produced by different bacteria, or that brGDGT producers in lakes respond differently to environmental changes than those in soils (Russell et al., 2018). Separation of the 5-methyl and 6-methyl brGDGTs yields slightly better error statistics for the East African lake calibration and lacks outliers such as are present in the calibration without separation of these isomers, re-affirming the potential of brGDGTs for paleotemperature reconstructions in lakes (Russell et al., 2018). Nevertheless, Weber et al. (2018) recently showed that variations in brGDGT composition above and below the oxycline in Lake Lugano (Switzerland) are linked to the occurrence of distinct bacterial groups that thrive in the oxic and anoxic parts of the water column. In addition, the carbon isotopic composition of brGDGTs in the sediments of Alpine lakes indicates that brGDGT producers are differentiated according to lake trophic status. Together, this suggests that brGDGT signatures in a lake sediment record may also be influenced by temperature-independent factors, such as variations in community composition and primary production (Weber et al., 2018).

In this study we examined brGDGTs in suspended particulate matter (SPM) from the water column of a permanently stratified lake (Lake Chala) in tropical Africa over a 17-month period to further constrain the seasonal and depth distribution of different brGDGTs, to identify their main producers, and to ascertain the sources of brGDGTs eventually stored in lake sediments. To this effect the SPM brGDGT data were compared with measurements of temperature, pH and dissolved oxygen (DO) obtained through concurrent water-column monitoring, and with the composition and abundance of bacterial taxa in the SPM based on 16S rRNA gene amplicon sequencing and quantification. We also analyzed brGDGTs in settling particles collected at monthly intervals over a 4.5-year (53-month) period, to reveal possible long(er)-term trends in the seasonality of brGDGT production in this lake, which may help elucidate its environmental drivers. Finally, comparison of the aquatic brGDGT signature with that of soils surrounding the lake and the lake sediments itself was expected to shed light on the significance of paleoclimate reconstructions based on brGDGTs in lake sediments.

2. Material and methods

2.1. Study system

Lake Chala (locally "Challa", after a nearby village) is a small (4.2 km^2), deep (~90 m) and permanently stratified (meromictic) crater lake, situated at ~880 m above sea level and bridging the border of Kenya and Tanzania (3°19'S, 37°42'E) in the foothills of Mt. Kilimanjaro. At this near-equatorial location, mean monthly air temperature (MMAT) varies between 21-22 ºC in July-August and 26-28 ºC in January-February (Buckles et al., 2014; Bodé et al., 2020). The tropical rain belt associated with latitudinal migration of the Inter-Tropical Convergence Zone (ITCZ) passes across the region twice yearly, resulting in two wet seasons and two dry seasons. Short rains occur from late October to December, and long rains from March to mid-May. The principal dry season occurs during southern hemisphere winter (June-September) and is characterized by lower air temperature and higher wind speeds. The latter drive evaporative cooling which promotes deep convective mixing of the water column of Lake Chala to ~40-60 m depth, while the deeper water remains permanently stratified and anoxic (Wolff et al., 2011; Buckles et al., 2014; van Bree et al., 2018). A second period of lesser mixing, to 25-30 m depth, occurs during the short dry season of January-February. Primary productivity is highest during the principal dry season (June to October), when nutrient-rich deep water is mixed upwards into the normally unproductive epilimnion (Wolff et al., 2014; van Bree et al., 2018). The lake's water balance is partly maintained by rainfall on the lake surface and over the steep-sloping crater basin, occasionally supplemented by high rainfall over the catchment of a small creek which breaches the north-western crater rim (Buckles et al., 2014). As lake-surface evaporation (1700 mm yr^{-1}) greatly exceeds annual rainfall (600 mm yr^{-1}), water balance is maintained by substantial subsurface inflow (Payne, 1970) of water that originates from percolation in or above the forest belt on Mt. Kilimanjaro (Hemp, 2006; Bodé et al., 2020).

2.2. Field observations and sample collection

2.2.1. Temperature, pH, and dissolved-oxygen monitoring of the water column

Vertical profiles of temperature, dissolved oxygen (DO), conductivity (K25) and pH were measured at 2-m intervals through the upper 50 m of the water column using a Hydrolab Quanta® multi-sensor probe at a mid-lake position (Fig. 2), at monthly intervals between September 2013 and January 2015 (van Bree et al., 2018). Additionally, water temperature was measured by automatic temperature loggers, at 2-hourly intervals between September

2010 and January 2015, suspended at a selection of the following water depths: 2, 10, 20, 25, 30, 35, 40, 45, 50 and 85 m. The set of monitoring depths varied over time due to the occasional malfunctioning and subsequent replacement of loggers. Due to loss of logger data during retrieval, no water-column temperature information is available for the period between 7 January and 11 September 2012. The entire 53-month temperature record was corrected for drift of individual loggers, using the Hydrolab profiles as reference. Periods of water-column mixing and stratification were determined on the basis of the temperature-logger time series, or estimated for the abovementioned hiatus period on the basis of mean monthly air temperature (MMAT) data from Bodé et al. (2020); the latter represents a savanna site ~25 km to the west of Lake Chala and at similar elevation.

2.2.2. Suspended particulate matter sampling

Collection of the SPM profiles used in this study has been described by van Bree et al. (2018). In short, 5 to 10 L of lake water was collected at 13 discrete depths, monthly between September 2013 and January 2015. The samples were filtered on pre-combusted glass fiber GF/F filters (142 mm diameter, Whatman), stored frozen, and freeze-dried prior to analysis. The SPM was collected at or near the start of every month as discussed here, with the sample taken at, for example, 07-09-2013 representing September 2013, and the sample taken at 30-09-2013 representing October 2013 (see Table S.1).

2.2.3. Sampling of settling particles

A sediment trap (UWITEC, double-funneled, 86 mm diameter) suspended in 35 m water depth at a mid-lake position (Fig. 2) was installed in November 2006, after which it was emptied and redeployed at about monthly intervals (Table S.1). The collected material was allowed to settle for two days, and stored frozen after decantation of excess water. Prior to analysis, the samples were thawed, filtered over pre-weighed and pre-combusted (400 ºC, 5 h) glass fiber GF/F filters (110 mm diameter, Whatman), then frozen and freeze-dried. Bulk mass flux was calculated for each month by using the dry weight of the collected particles, the number of days covered and the surface area of the sediment trap (58 cm^2), and is expressed as mg m^{-2} day^{-1}. This study focuses on the brGDGTs in settling particles representing the period from September 2010 until January 2015 (n = 53; Table S.2).

2.2.4. Soil sampling

Seven soil samples from the collection obtained by Buckles et al. (2014) were selected for brGDGT analysis based on site dissimilarity, i.e. from different origins (lakeshore forest, crater rim, savanna hinterland, small ravine; see Table S.3) as described in the original study.

2.2.5. Lake sediment sampling

Intact surficial lake-bottom sediment (2-5 cm depth) from 3 sites (CH10-06G: 3°19.049' S, 37°41.879' E; CH10-09G: 3°18.704' S, 37°41.448' E and CH10-10G: 3°18.575' S, 37°41.419' E; see Table S.4) forming a transect from close to the creek inlet towards the middle of the lake (Buckles et al., 2014) was collected by gravity coring in January-February 2010, then freeze-dried and homogenized prior to extraction.

2.3. Sample preparation and lipid extraction

Sample preparation for SPM was described in detail by van Bree et al. (2018). For this study, SPM was used from all depths for the months of November 2013 and August 2014, as well as from 0, 10, 25, 35, 50, 60, 70 and 80 m depth for all other months (total n = 146). In short, the freeze-dried filters were cut in small pieces and extracted using a modified Bligh-Dyer method. Each extract was acid-hydrolyzed with 1.5 N HCl in methanol (MeOH). After a 2 h reflux at 80 ºC, the pH of the hydrolyzed extract was adjusted to 4-5 by addition of 1 N KOH / MeOH (96%), and washed three times with dichloromethane (DCM). The combined organic phases were passed over a Na_2SO_4 column and dried under N_2. The total lipid extract (TLE) obtained was separated on an activated Al_2O_3 column into a-polar, neutral and polar fractions, using respectively hexane:DCM (9:1, v/v), DCM and DCM:MeOH (1:1, v/v) as eluents. The freeze-dried filters with sediment-trap material were cut in small pieces and extracted directly by acid hydrolysis. The obtained TLE was further processed in similar manner as the SPM TLE. The lake-sediment samples were also extracted and processed as the SPM.

A known amount of internal standard (99 ng C_{46} GDGT; Huguet et al., 2006) was added to the polar fraction of SPM, settling particles and sediments. All polar fractions of SPM, sediment trap, surface sediments and soils were re-dissolved in hexane:isopropanol (99:1, v/v), and then passed over a 0.45 μm PTFE filter.

2.4. GDGT analysis and proxy calculation

GDGT analysis was performed with an Agilent 1260 Infinity ultrahigh performance liquid chromatography (UHPLC) coupled to an Agilent 6130 single quadrupole mass detector, either

at Utrecht University (most SPM, soil, surface sediments) or at the NIOZ (settling particles, SPM at 0 m, except November 2013 and September 2014). The instruments at both laboratories are tuned towards the same standards and follow the method of Hopmans et al. (2016), in which separation is achieved by two silica Waters Acquity UPLC HEB Hilic (Ø 1.7 μm) columns at 30 °C, preceded by a guard column with similar packing. Isocratic elution was used for GDGT separation, starting with 82% A (hexane) and 18% B (hexane : isopropanol, 9:1) for 25 min at a flow rate of 0.2 mL min^{-1}, followed by a linear gradient to 70% A and 30% B for 25 min. Injection volume was 10 μL for settling particles, sediment and soils, and 20 μL for SPM. Ionization of the GDGTs was achieved by atmospheric pressure chemical ionization with gas temperature of 200 °C, vaporizer temperature of 400 °C, N_2 flow of 6 L min^{-1}, capillary voltage of 3500 V, nebulizer pressure of 25 psi and corona current of 5.0 μA as source conditions.

GDGTs were identified by detecting the $[M+H]^+$ ions in selected ion monitoring (SIM) mode for *m*/*z* 1018, 1020, 1022, 1032, 1034, 1036, 1046, 1048, 1050 (brGDGTs) and 744 (internal C_{46} GDGT standard). Peak area integration of the GDGTs was done with Chemstation (SPM, soil, sediment) or Agilent Masshunter (settling particles, SPM at 0, 35, 60 and 70 m) software. For quantification, areas were compared to that of the internal standard, assuming a comparable response of the mass spectrometer for all GDGTs. Fractional abundances of brGDGTs were calculated by dividing the peak area of a specific brGDGT divided by the peak areas of all measured brGDGTs.

The Roman numerals in the following equations refer to the molecular structures of GDGTs as shown in Fig. 1, with 6-methyl brGDGTs distinguished by an accent, and square brackets indicating the fractional abundances of the 15 different brGDGTs. The Cyclisation of Branched Tetraethers (CBT′) was defined by De Jonge et al. (2014b) as

$$CBT' = -\log \{([Ic] + [IIa'] + [IIb'] + [IIc'] + [IIIa'] + [IIIb'] + [IIIc']) / ([Ia] + [IIa] + [IIIa])\} \quad (1)$$

where [x] refers to the fractional abundance of a specific brGDGT.

The isomerization ratio of the 6-methyl penta- and hexamethylated brGDGTs over 5-methyl and 6-methyl brGDGTs (IR_{6ME}) was modified from De Jonge et al. (2014b) and Sinninghe Damsté (2016), and calculated as

297 IR_{6ME} = ([IIa′] + [IIb′] + [IIc′] + [IIIa′] + [IIIb′] + [IIIc′]) / ([IIa] + [IIb] + [IIc] + [IIIa] + [IIIb]
298 + [IIIc] + [IIa′] + [IIb′] + [IIc′] + [IIIa′] + [IIIb′] + [IIIc′]) (2)
299
300 Mean annual air temperature (MAAT) was reconstructed with the stepwise-forward-selection
301 (SFS) calibration of the brGDGT distribution in the East African lakes dataset (Russell et al.,
302 2018):
303
304 $MAAT_{SFS}$ = 23.81 – 31.02*[IIIa] – 41.91*[IIb] – 51.59*[IIb′] – 24.70*[IIa] + 68.80*[Ib] (3)
305
306 Surface-water pH was reconstructed with the Russell et al. (2018) transfer function
307 determined for East African lakes:
308
309 Surface water pH = 8.95 + 2.65*CBT′ (4)
310
311 **2.5. Determination of 16S rRNA gene diversity and abundance**
312 DNA was extracted from 1/32 section of the SPM filters using the PowerSoil DNA extraction
313 kit (Mo Bio Laboratories, Carlsbad, CA, USA). The 16S rRNA gene amplicon sequencing
314 and analysis was performed with the general 16S rRNA archaeal and bacterial primer pair
315 515F and 806RB targeting the V4 region (Caporaso et al., 2012), as described in Besseling et
316 al. (2018). PCR products were gel-purified using the QIAquick Gel-Purification kit (Qiagen),
317 pooled and diluted. Sequencing was performed at the Utrecht Sequencing Facility (Utrecht,
318 the Netherlands) using an Illumina MiSeq 2x300 bp sequencing platform. The 16S rRNA
319 gene amplicon sequences were analyzed by an in-house pipeline including quality assessment
320 by FastQC (Andrews, 2010), assembly of the paired-end reads with PEAR (Zhang et al.,
321 2013), and taxonomic assignment (including picking of a representative set of sequences with
322 the 'longest' method; Caporaso et al., 2010) with BLAST (Altschul et al., 1990) by using the
323 Silva 128 release as reference database (https://www.arb-silva.de/). The 16S rRNA gene
324 copies were quantified using quantitative PCR (qPCR) with the same primer pair (515F,
325 806RB) as used for amplicon sequencing. The 25 µl qPCR reaction mixture contained 1 U of
326 Pico Maxx high-fidelity DNA polymerase (Stratagene, Agilent Technologies, Santa Clara,
327 CA), 2.5 µl of 10x Pico Maxx PCR buffer, 2.5 µl of each dNTP at a concentration of 2.5 mM,
328 0.5 µl BSA at a concentration of 20 mg ml^{-1}, 0.02 pmol/µl of primers, Invitrogen SYBR
329 Green® (optimized concentration) diluted 10,000 times, 0.5 µl of 50 mM $MgCl_2$, and
330 ultrapure sterile water. The cycling conditions for the qPCR reaction were the following:

initial denaturation at 98 °C for 30 s, 45 cycles at 98 °C of 10 s each, pausing at 56 °C for 20 s followed by a plate read, then at 72 °C for 30 s, and finally at 80 °C for 25 s. Specificity of the reaction was tested with a gradient melting-temperature assay, from 55 °C to 95 °C with a 0.5 °C increment for 5 s. The qPCR reactions were performed in triplicate with standard curves from 100 to 107 molecules per microliter. qPCR efficiency for the 16S rRNA quantification was on average 95 % with $R^2 = 0.998$.

2.6 Statistical analysis

To assess variability in brGDGT distribution among (types of) samples we performed principal component analysis (PCA) in the R-package FactoMineR (Lê et al., 2008). For SPM, statistic analysis only used the fractional abundance of the most abundant brGDGTs, i.e., Ia, Ib, IIa, IIa′, IIb, IIb′, IIIa and IIIa′. Water temperature and pH were also included in the PCA, with pH between 50 and 90 m water depth assumed to be similar to the pH measured at 50 m depth. Although complete pH profiles from Lake Chala show that pH still decreases slightly with depth below 50 m (~0.5 pH units; Wolff et al., 2014), this represents only a quarter of the total pH depth gradient.

Concentrations of brGDGTs (ng L^{-1}) were correlated with the estimated abundance of microbial groups to assign a possible source of the former. The abundance of specific bacterial groups was estimated by multiplying their relative abundance as obtained by 16S rRNA gene amplicon sequencing analysis with the absolute abundance of microorganisms in a given sample based on qPCR. For simplicity it was assumed that each microbe contains a single 16S rRNA copy in their genome; the abundance was accordingly expressed as 16S rRNA gene copies L^{-1}. On the premise that potential brGDGT producers must be frequently present in the water column, microbial species present in less than 10% of the SPM samples were excluded from this comparison.

3. Results

3.1. Seasonal mixing and stratification

Surface-water temperature as measured by temperature loggers at 2 m depth, over the 29-month period from September 2012 to January 2015, ranged between 22.8 ºC during the mixing-season in August 2013 and 27.6 ºC during the period of strong stratification in April 2013 (Fig. 3). Temperatures at 10, 20 and 25 m depth, i.e. in lower epilimnetic and upper hypolimnetic water, varied seasonally with minima during the period of shallow mixing (SM;

January-February) and towards the end of the period of deep mixing (DM; May to mid-September). Seasonal temperature variation at 50 m depth, i.e. near the mixing limit, was already strongly muted, and at 85 m depth water temperature remained stable at ~22.4 ºC (Fig. 3), indicating lack of mixing. Over the 4.5-year monitoring period from September 2010 to January 2015 also the upper water column of Lake Chala developed stratification generally from September until April, with most strongly stratified conditions (i.e., greatest temperature contrast between the surface and deep water) shortly after the annual peak in local air temperature (February-March; Fig. 3).

During the 17-month period of lake monitoring between September 2013 and January 2015, the thickness of oxygenated upper part of the water column, as based on the depth to anoxia (shallowest depth with <0.2 mg L^{-1} dissolved oxygen), varied between 17 m in October-November 2013 and 44 m in October-November 2014 (Fig. 3). Depression of the oxycline resulted from convection-driven oxygen injection, mainly towards the end of the stratified period and throughout the principal mixing period. In contrast, the period of shallow mixing in January-February had little impact on the depth of the oxycline (Fig. 3).

3.2. Spatial and temporal distribution of brGDGTs in SPM

BrGDGTs were detected in all SPM samples analyzed (n = 143, Fig. 4). However, the abundance of brGDGTs with one or two cyclopentyl moieties (types b and c; Fig. 1) was often too low for reliable quantification (i.e., peak height less than three times the noise level of the baseline). Specifically, concentrations of brGDGTs IIIc and IIIc′ were always below detection limit; and brGDGTs Ic, IIc, IIc′, IIIb and IIIb′ were present in less than half of the SPM samples and in very modest amounts, often around the detection limit. The IIIa″ isomer (Weber et al., 2015), which has so far been detected only in lakes, was not detected at all in our samples. Consequently, in the following analysis we focus on the eight brGDGTs that were detected in at least 60% of the samples (i.e., Ia, Ib, IIa, IIa′, IIb, IIb′, IIIa and IIIa′) unless stated otherwise.

The total concentration of these eight brGDGTs in the water column (ΣbrGDGTs) varied between 0.2 and 24 ng L^{-1} (n = 143), and generally increased with depth, especially in the anoxic part of the water column (Fig. 4). The concentration-weighted mean fractional abundances of the individual brGDGTs in SPM collected at all depths above the sediment trap (0-35 m; $SPM_{abovetrap}$) and below it (40-90 m; $SPM_{belowtrap}$) over the 17-month sampling period are shown in Fig. 5A. Pentamethylated (type II) brGDGTs were the most common overall, with a summed fractional abundance ranging from 0.44 to 0.74 in the total dataset (n = 143)

and average values of 0.64 in $SPM_{abovetrap}$ (n = 72) and 0.72 in $SPM_{belowtrap}$ (n = 71). BrGDGT IIa′ was often dominant in the SPM of Lake Chala, with a fractional abundance ranging from 0.11 to 0.60, and average values for $SPM_{abovetrap}$ and $SPM_{belowtrap}$ of 0.56 and 0.57, respectively (Fig. 5A). The tetramethylated (type I) brGDGTs amount to between 0.06 and 0.47 of the brGDGT fractional abundance (n = 143), with average values of 0.31 in $SPM_{abovetrap}$) and 0.21 in $SPM_{belowtrap}$; brGDGT Ia is the second-most abundant of all brGDGTs (Fig. 5A). Finally, the concentration of hexamethylated (type III) brGDGTs is relatively variable with a combined fractional abundance between 0 and 0.25 (n = 143), where brGDGT IIIa′ is the most dominant compound. The hexamethylated brGDGTs have relatively low concentration-weighed average fractional abundances of 0.05 in $SPM_{abovetrap}$ and 0.08 in $SPM_{belowtrap}$. Overall the tetramethylated brGDGTs are relatively more common in the upper water column (fractional abundances $SPM_{abovetrap} > SPM_{belowtrap}$), whereas penta- and hexamethylated brGDGTs are relatively more abundant in the lower water column ($SPM_{abovetrap} < SPM_{belowtrap}$).

In >86% of all SPM samples, 6-methyl brGDGTs were more abundant than 5-methyl brGDGTs, which is reflected in an average IR_{6ME} of 0.74 (range 0.38 - 1.00). The 5-methyl brGDGTs were relatively abundant only between November 2013 and August 2014, with a maximal fractional abundance of 0.33 at 35 m in February 2014. Absolute concentrations of 5-methyl brGDGTs peaked at 8.0 ng L^{-1} at 60 m depth in April 2014. This is mainly the result of brGDGT-IIb, which contributed 4.8 ng L^{-1} to this amount (Fig. 4). The concentration of 6-methyl brGDGTs was typically highest in the non-mixing deepest part of the water column (>60 m), and reaches 9.3 ng L^{-1} at 80 m in February 2014 (Fig. 4). However, averaged over the sampling period the concentration-weighted fractional abundance of 6-methyl brGDGTs was quite similar in shallow and deep water, with an $SPM_{abovetrap}$ value of 0.62 and $SPM_{belowtrap}$ value of 0.66.

The concentrations of both ΣbrGDGT and individual brGDGTs were highest in the anoxic part of the Chala water column under stratified conditions (Fig. 4). Importantly, depth-integrated concentrations (i.e., averaged over the entire water column) were also highest during the stratification periods, and lowest towards the end of the deep-mixing period in 2014 when the oxycline was maximally depressed. Towards the end of both 2013 and 2014, brGDGT concentrations increased when stratification developed after the period of deep mixing. However, the two stratification periods differed with regard to the fractional abundance of individual brGDGTs. During stratification in 2013/2014, the brGDGT assemblage mainly consisted of Ib and IIb at 35-60 m water depth, and IIa′ and IIIa′ at 60-80

m, whereas during stratification in late 2014 and early 2015, concentrations of Ib and IIb were strongly reduced and notably high concentrations of IIa′ and IIIa′ were evident up to 25-35 m water depth (Fig. 4).

The first three principal components (PCs) of a principle component analysis (PCA) on the fractional abundances of the eight major brGDGTs in all SPM samples (n = 143) together explain 83.5% of the observed variation in their distribution (Figs. 6A-B). PC1 explains 49.4% of the variance, has strong negative loadings for the 6-methyl brGDGTs IIa′ and IIIa′, and strong positive loadings for the 5-methyl brGDGTs Ib, IIa, IIb and IIIa. PC2 explains 21.0% of the variance, and mainly shows strong negative loadings for Ia and IIb′. PC3 explains 13.1% of the variance and shows a strong positive loading for IIb′ and IIIa.

3.3. BrGDGTs in settling particles

The total brGDGT flux captured by the sediment trap at 35 m depth varied by two orders of magnitude (between 84 and 5300 ng m^{-2} day^{-1}) over the 53-month period of sediment-trap deployment (Fig. 7B). Total brGDGT flux is not related (R^2 = 0.02, p = 0.91) to the bulk flux of settling particles (Fig. 7A), nor does its production (or sedimentation) appear to be concentrated in a specific season. BrGDGT concentrations in the monthly collection of settled particles were generally higher than in the snap-shot SPM samples, enabling quantification of all studied brGDGTs except IIIc. Nevertheless, like in SPM, the fractional abundance of brGDGTs IIc, IIIb and IIIc′ was <0.02 at all times, and rarely >0.02 for Ic, IIc′, IIIa and IIIb′ (Fig. 5A). BrGDGTs IIc, IIIb and IIIc′ were also found in only 62-77% of the 53 trap samples, whereas all other brGDGTs were found in at least 94% of these samples.

The distribution of brGDGTs shows large variation throughout the period of settling particle collection (Figs. 7B-F). The majority of brGDGTs in settling particles were pentamethylated, with a combined fractional abundance ranging between 0.46 and 0.61 (n = 53), similar to what was found for SPM. BrGDGT IIa′ was again most often the dominant compound (fluxes of up to 3200 ng m^{-2} day^{-1} in November 2014; Fig. 5A), although at times IIb (340 ng m^{-2} day^{-1} in March 2014) and IIb′ (530 ng m^{-2} day^{-1} in August 2013) were also abundant in the settling particle flux. The fractional abundance of tetramethylated brGDGTs (mostly Ia, as in the SPM) ranged from 0.11 to 0.46, and hexamethylated brGDGTs (mostly IIIa′, as in the SPM) ranged from 0.07 to 0.28. Further, 6-methyl brGDGTs most often (41 out of 53 months) comprised at least 80% of the total 5- and 6-methyl brGDGTs (IR_{6ME} > 0.8), except in June 2011 and from November 2013 to September 2014 (Fig. 7C).

The first three PCs of the PCA on the fractional abundances of the eight brGDGTs most common in settling particles (Ia, Ib, IIa, IIa′, IIb, IIb′, IIIa and IIIa′, i.e. as in the SPM) together explain 91.4% of the observed variation through time (n = 53; Fig. 6C-D). PC1 explains 57.5% of the variance and has strong negative loadings for the 6-methyl brGDGTs IIa′ and IIIa′, and positive loadings for the 5-methyl brGDGTs Ia, Ib, IIa, IIb and IIIa. PC2 explains 23.7% of the total variance and has strong negative loadings for Ia and IIb′, and positive loadings for especially IIa, IIb and IIIa. PC3 explains 10.2% of the total variance and has a strong positive loading for Ia. Thus, variation in individual brGDGT distributions is overall similar in SPM and settling particles (cf. Figs. 6A-B and 6C-D).

The combined PCA on all 143 SPM and 53 sediment-trap samples (Fig. 6E) indicates that variation in brGDGT distributions is mainly structured by the relative abundance of 5- and 6-methyl brGDGTs (PC1 explains 48.6% of the total variance), and by a different behavior of brGDGTs Ia and IIb′ from the six other brGDGTs (PC2 explains 22.4% of the total variance). As expected, the brGDGT distribution in settling particles is most similar to that in SPM from the upper water column, i.e. sampled at depths situated above the sediment trap (Fig. 6E).

3.4. BrGDGTs in catchment soils

BrGDGTs in soils surrounding Lake Chala (n = 7) are predominantly tetramethylated (fractional abundance 0.48-0.84), followed by pentamethylated (0.15–0.44) and hexamethylated (0.01–0.09) compounds (Fig. 5B). Tetramethylated brGDGTs as well as compounds IIa′, IIb′ and IIIa′ were present in all analyzed soils. Several penta- and hexamethylated brGDGTs were below detection limit in two (IIa, IIIb), three (IIb), four (IIa′, IIIb′), five (IIIa) or all seven (IIIc, IIIc′) soil samples, and the fractional abundance of IIc, IIc′, IIIb and IIIb′ was usually <0.02 (Fig. 5A). The IR_{6ME} of Chala soils ranges between 0.52 and 0.90, with an average value of 0.73 (Fig. 7C). Variation in brGDGT distributions among soils is explained mainly by their location in- or outside of the crater basin (hinterland savanna, ravine, crater rim or lakeshore forest), in line with results of earlier analyses that did not differentiate between 5- and 6-methyl brGDGTs (Buckles et al., 2014). The brGDGT distributions in soils differ substantially from those in SPM and settling particles, mainly because of higher fractional abundances of brGDGTs Ia, Ib and IIa, and correspondingly lower proportions of 6-methyl brGDGTs (Fig. 5A). When soil brGDGT distributions are added to the PCA of water column brGDGTs as passive samples, all soils plot in the third

quadrant of positive PC1 and negative PC2 values, distinct from the lake SPM and settling particles (Fig. 6E).

3.5. BrGDGTs in surficial lake-bottom sediments

All brGDGTs except IIIc and IIIc′ were detected in recently deposited lake-bottom sediments (n = 3), although the fractional abundances of Ic, IIc, IIc′, IIIb and IIIb′ are always <0.02 (Fig. 5A). The distribution of individual brGDGTs is highly similar among the three analyzed samples (Figs. 5B and 6E), with fractional abundances of 0.47-0.48 for penta-, 0.40-0.41 for tetra-, and 0.12 for hexamethylated brGDGTs, and Ia (0.31) and IIa′ (0.27) being the dominant compounds. IR_{6ME} is ~0.67 (Fig. 7C). The brGDGT distribution in these lake sediments falls within the range of those found in SPM and settling particles (Fig. 5B), however with only positive PC1 scores (Fig. 6E).

3.6. Microbial diversity and abundance in the water column of Lake Chala

The diversity and abundance of prokaryotes in the water column of Lake Chala was determined by analysis of all collected SPM samples (n = 216), using Q-PCR and 16S rRNA gene amplicon sequencing. Proteobacteria formed the most important group of microbes but Acidobacteria, Actinobacteria, Chlorobi, Chloroflexi, Cyanobacteria, Firmicutes, Bacteriodetes, Planctomycetes, Parcubacteria, and Verrucomicrobia, were also present in varying relative amounts. The relative abundance of Acidobacteria reached a maximum of 4% but on average represented only 0.1% of the prokaryotic population (Table S.5). Among the Acidobacteria, sequences closely affiliated to Blastocatellia (subdivision (SD) 4), as well as those closely related to SD 21 and SD 6 dominated throughout the water column (Table S.5).

The absolute concentrations of the eight most common brGDGTs in the Lake Chala SPM are linked to the spatiotemporal distribution of specific bacterial groups based on 16S rRNA gene abundance estimates (Fig. 8). For Acidobacteria, a suspected phylum of brGDGT producers (Sinninghe Damsté et al, 2011), the highest degree of correlation was found between Acidobacteria SD 21 and brGDGTs Ib (R^2 = 0.23, $p < 0.001$, n = 132) and IIb (R^2 = 0.22, $p < 0.001$, n = 117). However, most correlations between individual brGDGTs and Acidobacteria SDs are weak ($R^2 < 0.15$; Fig. 8A). Outside the phylum Acidobacteria, modest positive correlations ($R^2 \geq 0.2$) were found between at least one of the eight major brGDGTs and the 16S rRNA gene abundance of 12 individual bacterial taxa (Fig. 8B). The highest positive correlation was found between brGDGT IIa and an uncultured bacterium of the phylum Aminicenantes (R^2 = 0.40, $p < 0.001$, n = 125).

4. Discussion

4.1. An aquatic origin of brGDGTs in Lake Chala

BrGDGTs in lakes can originate from both terrestrial and aquatic sources, and hence a mixed signal can be expected. There are several indications that the SPM of Lake Chala primarily contains brGDGTs produced within the water column rather than being washed in with eroding catchment soils. Firstly, at all times in the seasonal cycle brGDGT concentrations in the SPM show an order-of-magnitude increase with depth (Fig. 4). Based on data from a limited number of SPM profiles, it was previously thought that this pattern mainly originated because of favorable conditions for organic preservation in the anoxic lower water column of Lake Chala (Sinninghe Damsté et al., 2009; Buckles et al., 2014). Such a presumed stable brGDGT reservoir might be formed when slowly sinking organic particles become neutrally buoyant in the cooler hypolimnion and consequently accumulate over time, combined with a lack of processes (such as grazing and aggregation) to remove these particles from the water column (Sinninghe Damsté et al., 2009; Buckles et al., 2014). However, since our data also show significant variation in the distribution of individual brGDGTs between different depth intervals within the anoxic portion of the water column (Fig. 4), the concept of a static hypolimnetic brGDGT reservoir is untenable. Secondly, the depth-integrated total brGDGT concentration in SPM is lower at the end of the mixing season (and start of the ensuing stratification) than during peak stratification conditions (Fig. 4), arguing against the notion that upwelling during the mixing season merely disperses deep-water brGDGTs throughout the water column. Thirdly, the distribution and abundance of individual brGDGTs changes not only with depth but also through time (Fig. 4). Especially the changes in the lower water column are remarkable given the fact that the maximum mixing depth between September 2013 and January 2015 was limited to ~45 m (Fig. 3; van Bree et al., 2018). For example, the total brGDGT concentration at 80 m depth fluctuated between 0.98 ng L^{-1} (February 2014) and 16 ng L^{-1} (October 2014), and the different temporal trends of the individual brGDGTs result in variations in the degrees of cyclization, methylation, and 5- or 6-methyl positioning within the brGDGTs. Finally, the contrast between brGDGT distributions in soils and in SPM from either the oxygenated or anoxic parts of the water column (which largely correspond with the zones above and below the sediment trap; Fig. 5A-B), strongly suggests that high deep-water brGDGT concentrations do not result primarily from the accumulation of soil-derived brGDGTs preserved in anoxic conditions, but from *in situ* production, especially below the oxycline. Our combined evidence indicates that over the studied 17-month interval,

(almost) all brGDGTs in the SPM of the water column of Lake Chala have an aquatic source while terrestrial input is negligible. This result corroborates the findings of Buckles et al. (2014), and is also consistent with the general lack of terrestrial biomarkers, such as long-chain *n*-alkanes, in the SPM of Lake Chala during this same time interval (van Bree et al., 2018).

4.2. Spatiotemporal variation in brGDGT distributions

There is large variation in the fractional abundances of brGDGTs in the water column of Lake Chala over time. Under stratified conditions from November 2013 to August 2014, the expanded anoxic zone is characterized by high fractional abundances of brGDGTs Ib and IIb, which both peak in abundance at 60 m depth (Fig. 4). Although seemingly similar environmental conditions occurred at the end of 2014, when after the end of seasonal deep mixing the oxycline moved upwards again, the concentrations of Ib and IIb do not return to their earlier levels. Instead, concentrations of IIa′ and IIIa′ rapidly increase at this time. Hence, it appears that deeper mixing promotes either the production of Ib+IIb (5-methyl brGDGTs with rings), as observed in late 2013 and early 2014, or of IIa′+IIIa′ (6-methyl brGDGTs with no rings but additional methylation), as observed in late 2014. This temporal variation in brGDGT composition is captured by PC1 in the PCA, which clearly separates 5- and 6-methyl brGDGTs (PC1 49.4%; Fig. 6A). Moreover, the associated alternation of brGDGTs with and without cyclopentyl moieties is reflected by PC2 (Fig. 6A-B). Notably, where 5-methyl brGDGTs mostly occur between 35-60 m depth, 6-methyl brGDGTs generally reside in the lowermost portion of the water column (60-80 m; Fig. 4). Also 5- and 6-methyl brGDGTs with cyclopentyl moieties (Ib and IIb vs IIb') occur in different parts of the water column (Fig. 4). Although the concentrations of IIb′ in SPM are overall quite low, this depth segregation suggests that the incorporation of cyclopentyl moieties into 5-methyl and 6-methyl brGDGTs is driven by different factors.

4.3. Membrane plasticity *vs* community changes in aquatic brGDGT producers

It is generally assumed that brGDGT producers adjust the molecular structure of their membrane lipids in response to environmental changes, and in fact, these membrane adaptations are at the heart of brGDGT-based paleoenvironmental proxies (e.g. Weijers et al., 2007b). In general, the distribution of individual brGDGTs in the SPM of Lake Chala is in line with the ambient environmental conditions. Overall dominance of the 6-methyl brGDGTs (Fig. 5) may be associated with the relatively high pH of the lake (8.2-9.3 at the surface;

599 Wolff et al., 2014), given that 6-methyl brGDGTs are predominantly produced under high-pH
600 conditions in soils (De Jonge et al., 2014a) as well as river (De Jonge et al., 2014b) and lake
601 (Russell et al., 2018) water. Also the relatively low abundance of hexamethylated (both 5- and
602 6-methyl) brGDGTs is characteristic for warm lakes (Tierney et al., 2010; Loomis et al.,
603 2014a; Russell et al., 2018). However, in Lake Chala there is no straightforward link between
604 brGDGT distributions and the seasonal cycle of environmental conditions, as illustrated by
605 the distinct brGDGT distributions in the two episodes of strong stratification during our 17-
606 month study period, and by the apparently different drivers of cyclization in 5-methyl versus
607 6-methyl brGDGTs (see section 4.2). The fact that temporal variation in the fractional
608 abundance of aquatically produced brGDGTs is not easily linked to the seasonal cycle in
609 either temperature, dissolved oxygen distribution, or pH suggests that the brGDGT molecular
610 structure is not primarily governed by membrane adaptation to changing abiotic conditions.
611 Instead, they may result from variation in the composition of the lake's bacterial community,
612 which, if the different bacterial taxa produce different brGDGTs, will result in different
613 brGDGT assemblages at different times. This was also observed in the deep and meromictic
614 Lake Lugano (Switzerland), where compositional changes in brGDGTs with depth are
615 strongly related to bacterial community changes across the oxycline (Weber et al., 2018).
616 The producers of aquatic brGDGTs in Lake Chala can potentially be identified by
617 comparing the depth distribution and temporal variation of individual brGDGTs with 16S
618 rRNA gene data obtained from the same SPM samples, following the approach of Weber et
619 al. (2018) and Sollai et al. (2019). The only mesophilic bacteria currently known to produce
620 the assumed precursor lipids for brGDGTs, namely *iso*-diabolic acid and its 5- and 6-
621 methylated derivatives, are Acidobacteria (Sinninghe Damsté et al., 2011a, 2018). However,
622 their presence has only been demonstrated in soil-derived aerobic Acidobacterial strains
623 belonging to SDs 1, 3, 4, and 6, while strains of SDs 8, 10 and 23 do not contain these lipids.
624 Ether-bound *iso*-diabolic acid and its derivatives occur only in high abundance in SD4
625 (Sinninghe Damsté et al., 2011a, 2018). Small amounts of ether-bound *iso*-diabolic acid and
626 its derivatives, including brGDGT Ia, have been detected in two Acidobacteria SD1 species
627 isolated from soil. So far, only SD4 species have been shown to produce 5-methyl *iso*-
628 diabolic acid derivatives, whereas the other SDs formed 6-methyl *iso*-diabolic acids. This
629 suggested that the position of methylation of *iso*-diabolic acid may be controlled by
630 phylogenetic affiliations within the Acidobacteria and thus may not be a direct response to
631 ambient environmental conditions (Sinninghe Damsté et al., 2018). Only little is known about
632 the occurrence and diversity of Acidobacteria in lakes (e.g., Zimmermann et al., 2012;

633 Parvenova et al., 2016; Preheim et al., 2016), but the concentrations of some individual
634 brGDGTs in Lake Lugano at one instance during the seasonal cycle (in contrast to the
635 prolonged monthly sampling realized here) showed a strong empirical correlation ($R^2 > 0.56$)
636 with the abundance of certain Acidobacteria SDs (i.e. 3, 5, 6, 8, 15, 17, 21; Weber et al.,
637 2018).
638 In our data from Lake Chala, individual brGDGTs are only modestly correlated with
639 Acidobacteria SDs (Fig. 8A). Surprisingly, whereas in Lake Chala the concentration of
640 brGDGTs Ib and IIb correlates with the abundance of SD21 Acidobacteria, in Lake Lugano
641 this same SD correlates instead with the concentrations of brGDGTs IIa, IIIa and IIIa″ (Weber
642 et al., 2018). The weaker correlation observed in Lake Chala may be partly due to the method
643 of analysis; in contrast to the studies of Weber et al. (2018) and Sollai et al. (2019) we
644 determined the sum of core and intact polar lipid-derived individual brGDGTs rather than the
645 intact polar lipids separately. Intact polar lipids are generally considered to be better markers
646 for 'live' bacteria because the polar head group is thought to be lost quickly after cell death
647 (White et al., 1979; Harvey et al., 1986). However, given the overall low abundance of
648 Acidobacterial 16S rRNA sequences in Lake Chala SPM (on average 0.2% of total
649 prokaryotes, with values up to 6%), the omnipresence and high concentrations of brGDGTs
650 (Fig. 4), and the mostly weak correlation between them, it seems unlikely that Acidobacteria
651 are the predominant producers of brGDGTs in Lake Chala.
652 To investigate alternative bacterial sources for the brGDGTs, we also correlated their
653 individual concentrations with those of the bacterial taxa identified in the SPM (Fig. 8B).
654 Although empirical co-occurrence of brGDGTs and microbial taxa alone does not suffice to
655 reveal the exact source organism(s) of those brGDGTs, the detected phyla might either
656 contain brGDGT-producing organisms or be associated with similar habitats. For example,
657 correlation of brGDGT Ib and IIb with the Actinobacteria phylum may be indicative of the
658 depth habitat or growth season of the organism producing these specific brGDGTs. Our broad
659 brGDGT-16S rRNA data comparison clusters different groups of brGDGTs, and can broadly
660 be defined as Ib+IIb, non-cyclic 5-methyl brGDGTs, and 6-methyl brGDGTs, which all relate
661 to a different bacterial composition (Fig. 8B). The clustering is consistent with the
662 spatiotemporal alternation of brGDGTs Ib+IIb and IIa′+IIIa′ observed in the water column of
663 Lake Chala (Fig. 4), and suggests that these different brGDGTs (i.e., 5-methyl *vs* 6-methyl,
664 and cyclic *vs* non-cyclic brGDGTs) may be produced by different (groups of) bacteria.
665 Despite our extensive SPM dataset, it is at this stage not possible to determine exactly which
666 aquatic bacteria produce the brGDGTs in Lake Chala but the higher correlations with

667 bacterial taxa other than Acidobacteria suggests that an exclusive origin of lacustrine
668 brGDGTs by Acidobacteria is deemed unlikely, in agreement with earlier work (Weber et al.,
669 2018).
670
671 **4.4. Congruence between brGDGT distributions in SPM and settling particles**
672 It was previously noted that Lake Chala SPM is deprived of terrestrial biomarkers (van Bree
673 et al., 2018), whereas they do occur in the lake's bottom sediments (e.g., Sinninghe Damsté et
674 al., 2011b). Since the brGDGTs associated with SPM appear to be produced within the water
675 column, a possible contribution of soil-derived brGDGTs to the lake sediments may be
676 recognized in settling particles collected monthly in the sediment trap at 35 m, which
677 represents a depth- and time-integrated signal of the upper water column (although the trap is
678 located above the predominant zone of aquatic brGDGT production; Fig. 4). The 53-month
679 sediment-trap record fully encompasses our 17-month SPM time series and thus enables
680 direct comparison between the datasets. Notably, the brGDGT distribution in sediment-trap
681 material is highly similar to that in the SPM, both during the overlapping time period and
682 averaged over the 53-month interval, and dissimilar from the brGDGT distribution in
683 catchment soils (Figs. 5A and 6E). It thus appears that also the vast majority of brGDGTs in
684 particles settling through the water column has an aquatic origin, and consequently can be
685 expected to show the same temporal trends as the brGDGTs in SPM. Indeed, the observed
686 alternation in the summed fractional abundances of brGDGTs Ib+IIb versus IIa′+IIIa′ in SPM
687 can also be recognized in the settling particles (Fig. 7D-E). Onset of upper water-column
688 stratification is marked by the relative increase of one of these two groups: the fractional
689 abundance of IIa′+IIIa′ increased sharply at the onset of stratification in late 2010, 2012 and
690 2014, whereas those of Ib+IIb increased in late 2011 and 2013. The similar behavior of
691 brGDGTs in SPM and settling particles is also reflected in the PCA including both sample
692 series (Fig. 6E), where PC1 separates 5- and 6-methyl brGDGTs resulting from the temporal
693 alternation of Ib+IIb and IIa′+IIIa′. Although it is not clear which environmental variable
694 controls the predominance of either group in any one year, this pattern supports our
695 suggestion that changing brGDGT distributions in Lake Chala primarily reflect distinct
696 seasonal and inter-annual variation in the composition of its aquatic microbial community
697 rather than a physiological response in a compositionally stable resident community.
698 Notwithstanding their apparently similar dynamics, the sediment-trap and SPM time
699 series are not fully equivalent. The brGDGTs in settling particles are supposedly produced in
700 the upper 35 m of the water column, and indeed mostly plot with the $SPM_{abovetrap}$ samples in

701 the PCA (Fig. 6E). However, for the overlapping 17-month period the time-integrated
702 brGDGT distribution in sediment-trap material appears more similar to the abundance-
703 weighted, depth- and time-integrated brGDGT signal in SPM from the mostly anoxic water
704 column below the sediment trap (> 35 m) than to that of the more oxic upper water column (<
705 35 m; Fig. 5A-B). This suggests that a substantial contribution of brGDGTs to the sediment
706 trap may occur during periods when the oxycline is situated well above 35 m. In addition,
707 material from deeper water layers can also reach the sediment trap during mixing episodes
708 (reaching down to *ca* 40-45 m in 2014, and to as much as 60 m in other years; Verschuren et
709 al., 2009).
710 Temporal variation in brGDGT concentrations in the Lake Chala SPM appears to
711 respond mainly to the seasonal cycle of stratification and mixing (Fig. 4). This pattern is not
712 reflected in the 4.5-year sediment-trap record, where fluxes of both settling particles as a
713 whole and brGDGTs do not show a clear, recurring annual pattern (Fig. 7A-B). Substantial
714 temporal variation in the total flux and distribution of brGDGTs in Lake Chala has been
715 reported previously, based on analysis of settling particles collected monthly between
716 November 2006 and August 2010 (Sinninghe Damsté et al., 2009; Buckles et al., 2014). This
717 contrasts with findings from sediment-trap studies in north-temperate lakes (e.g. Loomis et
718 al., 2014b; Miller et al., 2018), where brGDGT distributions in settling particles remain
719 relatively stable despite large seasonal variation in their fluxes. Aside from the large temporal
720 variation in brGDGT distributions in Lake Chala, the whole of our 17-month SPM sampling
721 period, and the period from September 2013 to September 2014 in particular, stand out in the
722 53-month sediment-trap record due to the relatively high flux of 5-methyl brGDGTs with
723 rings (Ib+IIb), and relatively low flux of 6-methyl brGDGTs (IIa′+IIIa′) (Fig. 7D-E). The
724 relatively large contribution of 5-methyl brGDGTs during this period is reflected in low IR_{6ME}
725 values (< 0.7), otherwise uncommon in the entire 53-month time series (Fig. 7C). Notably,
726 this 13-month period of low IR_{6ME} is also characterized by the near-absence of terrestrial plant
727 biomarkers in the SPM (van Bree et al., 2018), which may indicate that this distinct brGDGT
728 signature is representative of a primarily aquatic source of the brGDGTs. Indeed, any
729 contribution of soil-derived brGDGTs would be revealed by increased abundance of
730 brGDGT-Ia, the dominant brGDGT in Chala catchment soils (Buckles et al., 2014; Fig. 5A).
731 However, the fractional abundance of brGDGT-Ia remains relatively stable over the entire 53-
732 month study period (Fig. 7F), implying that the vast majority of the brGDGTs in the
733 sediment-trap record have an aquatic origin. The caveat is that due to the mid-lake position of
734 the sediment trap and steeply sloping crater walls, we cannot exclude the possibility for soil

material to be deposited on the lake floor without reaching the sediment trap. This scenario may also explain the contrasting occurrence of terrestrial biomarkers in surficial bottom sediments and the water column (i.e., SPM) of Lake Chala.

4.5 Discrepancy between brGDGT signatures in the water-column, soils, and sediments

The brGDGT distribution in bottom sediments of Lake Chala clearly differs from those in the SPM and settling particles, even when distributions in the latter are integrated over time and weighted-averaged (Fig. 7C-F). For example, the full range of IR_{6ME} values is very wide in SPM (0.35-1.00) and settling particles (0.45-1.00) whereas the three sediment samples have near-identical IR_{6ME} values (~0.67) that are substantially lower than the overall weighted-average IR_{6ME} of the SPM and the settling particles (Fig. 7C). In other words, over 88% (n = 17) or 96.2% (n = 53) of brGDGTs II and III in SPM and settling particles belong to the 6-methyl variety (Fig. 7B), whereas this is only 67% in the bottom sediment. Also the brGDGT fractional abundances in the sediments are different from those in the water column, and in particular those of the 5-methyl brGDGTs without cyclopentane moieties (Ia, IIa, IIIa; Figs. 5 and 7). Interestingly, the sedimentary brGDGT signature is also clearly different from that of the catchment soils (Figs. 5 and 7). Although this may be the result of mixed aquatic and soil-derived brGDGTs, this cannot explain the fractional abundances of in particular brGDGT-IIa and IIb in the sediment, which are higher than those in both the water column and the soils (Fig. 5A). These differences in brGDGT signatures in the soils, water column and the sediment suggest that additional brGDGT production may take place within the bottom sediments, as suggested previously (Buckles et al., 2014). Hence, the final brGDGT signal that is stored in Lake Chala sediments is influenced by i) seasonal changes and substantial inter-annual variability in aquatic brGDGT production in the water column, ii) production within the sediments, and iii) varying proportions of aquatic and terrestrial brGDGTs over time, although the evidence for a soil contribution to Lake Chala sedimentary GDGTs remains weak.

4.6. Implications for brGDGT-based paleoclimate reconstruction

In order to use brGDGTs extracted from lake sediments for paleoclimate reconstruction, we need to understand how the environmental parameters of interest (primarily temperature and pH) are reflected by the signal that is finally exported to and preserved in the sedimentary record. An earlier study of brGDGTs in time series of settling particles from Lake Chala (Buckles et al., 2014) indicated that mean annual air temperature (MAAT) was

underestimated by ~11-13 °C (estimates were 14±5 ºC and 13±6 ºC, using the East African Lake (EAL) calibrations of Tierney et al. (2010) and Loomis et al. (2012), respectively). Furthermore, maxima and minima in reconstructed temperatures from the time series of settling particles lagged changes in air temperature by up to 5-6 months. Buckles et al. (2014) attributed these offsets to a shifted ratio of aquatic versus soil-derived brGDGTs, and also noted that the brGDGTs in Lake Chala may have a different relationship with temperature than those in the EAL calibrations. Moreover, the co-elution of 5- and 6-methyl brGDGTs in their analysis may have contributed to the observed offset. Application of the improved chromatography method (Hopmans et al., 2016) in the current study allows us to use the most recent temperature calibration based on stepwise forward selection of 5- and 6-methyl brGDGTs in the EAL dataset ($MAAT_{SFS}$; Russell et al., 2018). Application of this transfer function to our sediment-trap record generates MAAT estimates between 18.5 and 25.2 ºC (on average 22.1±1.7 ºC), and a flux-weighted overall average of 22.8 ºC (Fig. 7G). Underestimation of the observed local MAAT (24.5 ºC) is thereby reduced to about 2 ºC, i.e. in the range of the calibration error of 2.1 ºC.

Nevertheless, seasonal variation in reconstructed temperature based on settling particles does not seem very consistent (Fig. 7G). Whereas highest air (and surface-water) temperature occurs during the period of strong water-column stratification, brGDGT-based temperature inferences peak during the periods of stratification in 2010-2011, 2013-2014 and at the end of 2014, but also during the periods of deep mixing in 2011 and 2012 (Fig. 7G). As the temporal variation in brGDGT distributions in the water column of Lake Chala appears to be linked to microbial community changes that are at best only indirectly related to temperature, this may be one reason why brGDGT signatures do not clearly track measured MMAT (Fig. 7G). On the other hand, the modestly higher temperature of the epilimnion compared to that of the lower water column (up to ~4 °C, depending on the season) is reflected in a higher average reconstructed temperature for $SPM_{abovetrap}$ (23.4 ºC, $n = 72$) than $SPM_{belowtrap}$ (21.5 ºC, $n = 71$, $p < 0.01$; Fig. 7G). Similarly, the decrease of lake-water pH with depth (Wolff et al., 2014; van Bree et al., 2018) is reflected by higher reconstructed pH for the lake surface water (on average 8.5 at 0 m) than that of deeper water layers (on average 8.1 at 80 m; $p < 0.01$). Also the elevated surface-water pH that may be expected to occur during peak primary productivity in the mixing season appears to be recorded by brGDGTs in settling particles (8.1 during mixing ($n = 16$) versus 7.7 during stratification ($n = 37$; $p < 0.02$), even though the 53-month time series of brGDGT-inferred pH does not follow clear seasonal trends (Fig. 7H). Especially during the interval from September 2013 to September

803 2014 that is characterized by lower IR_{6ME} values, the inferred pH is nearly constant (as is,
804 incidentally, the observed pH: Fig. 7H). This low IR_{6ME} is the net result of the relative
805 increase in cyclopentane moieties (Ib+IIb, Fig. 7F) and decrease in the degree of
806 isomerization (more 5-methyl brGDGTs, Fig. 7C), whereas they are both positively related to
807 pH at least in global soils (Weijers et al., 2007; De Jonge et al., 2014). The opposite trends in
808 the degrees of cyclisation and isomerization of brGDGTs in settling particles of Lake Chala
809 also may explain the generally weak relationship between bottom-sediment brGDGT
810 distribution and surface-water pH in the EAL dataset (Tierney et al., 2010; Loomis et al.,
811 2014; Russell et al., 2018), and supports the suggestion made by these authors that an
812 environmental variable other than pH is responsible for changes in brGDGT signatures in
813 lakes.
814 Notably, average MAAT and pH values inferred from the brGDGTs in surficial
815 bottom sediments are yet again different from those based on brGDGTs produced in the water
816 column and in catchment soils (Fig. 7G, H). The distinct signature of the sedimentary
817 brGDGTs (Fig. 5A) suggests that besides an aquatic source and a potential, but unlikely, soil
818 contribution, those brGDGTs are partly produced within the sediment. However, although
819 brGDGT signals in lake sediments are generally, but not systematically, characterized by
820 larger proportions of hexamethylated brGDGTs and compounds with cyclopentane moieties
821 than those in catchment soils (Tierney and Russel, 2009; Sinninghe Damsté et al., 2009;
822 Tierney et al., 2010; Loomis et al., 2014b; Miller et al., 2018; Guo et al., 2020), it is still not
823 possible to determine the exact contributions of the different potential brGDGT sources to the
824 brGDGT signature stored in the sediments of a lake. This is in contrast to rivers and the
825 coastal marine environment, where *in situ* brGDGT production can be quantified on the basis
826 of the relative abundance of 6-methyl brGDGTs (De Jonge et al., 2014b) or the weighed
827 number of rings in the tetramethylated brGDGTs (Sinninghe Damsté, 2016). Regardless, the
828 values of MAAT (21.9 ºC) and pH (9.1) inferred from sedimentary brGDGTs in Lake Chala,
829 as generated using the most recent EAL calibration (Russell et al., 2018), are within
830 reasonable range of measured MAAT (24.5 ºC) and surface water pH (9.0). This result is
831 consistent with the belief that brGDGTs in lake sediments carry truthful environmental
832 information (e.g., Tierney et al., 2010; Russell et al., 2018), albeit indirectly, and suggests that
833 the available brGDGT-temperature calibrations already take the *in-situ* sedimentary
834 production into account. If this principle holds over longer timescales, it implies that we can
835 use brGDGTs in lake sediments for paleoclimate reconstructions, even without fully
836 understanding the mechanism that determines their signature. Nevertheless, given the lack of

837 an obvious link between brGDGT composition (or flux) in the 53-month record of settling
838 particles and observed MMAT indicates that sediment samples used for temperature
839 reconstruction must integrate over multiple years.
840

841 ## 5. Conclusions

842 BrGDGTs in the water column of Lake Chala are primarily produced *in situ*. The amounts
843 and distributions of individual aquatic brGDGT compounds are highly variable with depth
844 and over time, and do not consistently relate to ambient temperature, pH or oxygen but still
845 appear to respond to the seasonal alternation of water-column mixing and stratification, which
846 is under climatic control. The aquatic brGDGT assemblage is alternatively dominated by the
847 compounds Ib+IIb and IIa′+IIIa′, with each pair linked to the occurrence of different bacterial
848 taxa, other than, or besides the Acidobacteria. Hence, temporal changes in brGDGT
849 assemblages are likely due to the sequential occurrence of different groups of aquatic bacteria
850 producing different types of brGDGTs, rather than by membrane adaptation within one group.
851 BrGDGTs in settling particles reveal substantial inter-annual variation in the bacterial
852 community of this tropical lake, superimposed on seasonal variation. Although the brGDGT
853 distributions in SPM and settling particles from Lake Chala cannot be directly linked to local
854 variation in air or water temperature, temporally-integrated and flux-weighted brGDGT
855 compositions do produce reasonable temperature and surface-water pH estimates when using
856 the new EAL calibration of Russell et al. (2018). Regardless, the distinct brGDGT signature
857 of surficial bottom sediments suggests that part of the sedimentary brGDGT pool is produced
858 within the sediment itself. It thus remains crucial to discover the producers of brGDGTs, and
859 the general drivers of brGDGT production, in lakes so that the uncertainties in lacustrine
860 paleothermometry can be further constrained.
861

862 ## Acknowledgements

863 We thank C.M. Oluseno for conducting the monthly lake sampling and monitoring. We thank
864 A. Negash and P. de Regt for lipid extractions, and J.W. de Leeuw for feedback on the
865 manuscript. We are grateful to A. van Dijk, D. Kasjaniuk, A. van Leeuwen-Tolboom and K.
866 Nierop at Utrecht University; and M. Baas, D. Dorhout, E.C. Hopmans, A. Mets, J. Ossebaar,
867 S. Vreugdenhil and M. Brouwer at the Royal NIOZ for technical and analytical support. We
868 furthermore thank A. Roepert for help with R, and C. De Jonge for discussions on brGDGTs.
869 Comments of two anonymous reviewers have helped to further improve this manuscript.

870 Fieldwork with collection of the studied sample materials was carried out with permission
871 from the government of Kenya through permit 13/001/11C to D.V. In accordance with
872 National Environmental Management Authority regulations in the context of the Nagoya
873 Protocol, DNA extracts of the analyzed suspended-particulate samples are archived at the
874 National Museums of Kenya (NMK), under voucher numbers NMK:BCT:80001 to
875 NMK:BCT:80221; we thank A. Mwaura and S.M. Rucina for facilitation. The raw data of the
876 16S rRNA gene amplicon reads were deposited in the NCBI Sequence Read Archive (SRA);
877 BioProject number upon request. This research was supported by the NESSC Gravitation
878 Grant (024.002.001) from the Dutch Ministry of Education, Culture and Science (OCW) and
879 the European Research Council (ERC) under the European Union's Horizon 2020 research
880 and innovation program (grant agreement no. 694569 – MICROLIPIDS) both to J.S.S.D.

References

Altschul S. F., Gish W., Miller W., Myers E. W. and Lipman D. J. (1990) Basic local alignment search tool. J. Mol. Biol. 215, 403–410. doi.org/10.1016/S0022-2836(05)80360-2

Andrews S. (2010) A quality control tool for high throughput sequence data. http://www.bioinformatics.babraham.ac.uk/projects/fastqc/.

Bechtel A., Smittenberg R. H., Bernasconi S. M. and Schubert C. J. (2010) Distribution of branched and isoprenoid tetraether lipids in an oligotrophic and a eutrophic Swiss lake: insights into sources and GDGT-based proxies. Org. Geochem. 41, 822–832.

Besseling M. A., Hopmans E. C., Boschman R. C., Sinninghe Damsté J. S. and Villanueva L. (2018) Benthic archaea as potential sources of tetraether membrane lipids in sediments across an oxygen minimum zone. Biogeosciences, 15, 4047-4064.

Blaauw M., van Geel B., Kristen I., Plessen B., Lyaruu A., Engstrom D. R., van der Plicht J. and Verschuren D. (2011) High-resolution ^{14}C dating of a 25,000 year lake-sediment record from equatorial East Africa. Quat. Sci. Rev. 30, 3043-3059.

Bodé S., De Wispelaere L., Hemp A., Verschuren D. and Boeckx P. (2020) Water-isotope ecohydrology on Mt. Kilimanjaro. Ecohydrology 13, e2171.

Buckles L. K., Weijers J. W. H., Verschuren D. and Sinninghe Damsté J. S. (2014) Sources of core and intact branched tetraether membrane lipids in the lacustrine environment: anatomy of Lake Challa and its catchment, equatorial East Africa. Geochim. Cosmochim. Acta 140, 106–126.

Buckles L. K., Verschuren D., Weijers J. W., Cocquyt C., Blaauw M. and Sinninghe Damsté J. S. (2016) Interannual and (multi-) decadal variability in the sedimentary BIT index of Lake Challa, East Africa, over the past 2200 years: assessment of the precipitation proxy. Clim. Past. 12, 1243-1262.

Caporaso J. G., Kuczynski J., Stombaugh J., Bittinger K., Bushman F. D., Costello E. K. et al. (2010) QIIME allows analysis of high-throughput community sequencing data. Nature Meth. 7, 335–336.

Caporaso J. G., Lauber C. L., Walters W. A., Berg-Lyons D., Huntley J., Fierer N., Owens S. M., Betley J., Fraser L., Bauer M. and Gormley N. (2012) Ultra-high-throughput microbial community analysis on the Illumina HiSeq and MiSeq platforms. ISME J. 6, 1621.

913 Castañeda I. S. and Schouten S. (2011) A review of molecular organic proxies for examining
914 modern and ancient lacustrine environments. Quat. Sci. Rev. 30, 2851-2891.
915 Chevalier M., Chase B.M., Quick L.J., Dupond L.M. and Johnson, T.C. (2020) Temperature
916 change in subtropical southeastern Africa during the past 790,000 yr. Geology, in
917 press. doi: 10.1130/G47841.1
918 Colcord D. E., Cadieux S. B., Brassell S. C., Castañeda I. S., Pratt L. M. and White J. R.
919 (2015) Assessment of branched GDGTs as temperature proxies in sedimentary records
920 from several small lakes in southwestern Greenland. Org. Geochem. 82, 33–41.
921 Colcord D. E., Pearson A. and Brassell S. C. (2017) Carbon isotopic composition of intact
922 branched GDGT core lipids in Greenland lake sediments and soils. Org. Geochem.
923 110, 25-32.
924 Dearing Crampton-Flood E., Tierney J.E., Peterse F., Kirkels F.M.S.A. and Sinninghe Damsté
925 J.S. (2020) BayMBT: A Bayesian calibration model for branched glycerol dialkyl
926 glycerol tetraethers in soils and peats. Geochim. Cosmochim. Acta. 268, 142-159.
927 De Jonge C., Hopmans E. C., Stadnitskaia A., Rijpstra W. I. C., Hofland R., Tegelaar E. W.
928 and Sinninghe Damsté, J. S. (2013) Identification of novel penta- and hexamethylated
929 branched glycerol dialkyl glycerol tetraethers in peat using HPLC–MS, GC–MS, and
930 GC–SMB-MS. Org. Geochem. 54, 78–82.
931 De Jonge C., Hopmans E. C., Zell C. I., Kim J.-H., Schouten S. and Sinninghe Damsté J. S.
932 (2014a) Occurrence and abundance of 6-methyl branched glycerol dialkyl glycerol
933 tetraethers in soils: Implications for paleoclimate reconstruction. Geochim.
934 Cosmochim. Acta 141, 97–112.
935 De Jonge C., Stadnitskaia A., Hopmans E. C., Cherkashov G., Fedotov A. and Sinninghe
936 Damsté J. S. (2014b) *In situ* produced branched glycerol dialkyl glycerol tetraethers in
937 suspended particulate matter from the Yenisei River, Eastern Sibera. Geochim.
938 Cosmochim. Acta 125, 476–491.
939 Diefendorf A. F. and Freimuth E. J. (2017) Extracting the most from terrestrial plant-derived
940 *n*-alkyl lipids and their carbon isotopes from the sedimentary record: A review. Org.
941 Geochem. 103, 1-21.
942 Freeman K. H. and Pancost R. D. (2013) Biomarkers for terrestrial plants and climate. In:
943 Treatise on Geochemistry, Elsevier Inc., Second Edition, 395-416.
944 Guo J., Glendell M., Meersmans J., Kirkels F., Middelburg J.J. and Peterse F. (2020)
945 Asessing branched tetraether lipids as tracers of soil organic carbon transport through
946 the Carminowe Creek catchment (southwest England). Biogeosciences 17, 3183-3201.

947 Harvey, H.R., Fallon, R.D., and Patton, J.S. (1986) The effect of organic matter and oxygen
948 on the degradation of bacterial membrane lipids in marine sediments. Geochim.
949 Cosmochim. Ac. 50, 795-804.
950 Hemp A. (2006) Continuum or zonation? Altitudinal gradients in the forest vegetation of Mt.
951 Kilimanjaro. Plant Ecol. 184, 27-42.
952 Hopmans E.C., Schouten S. and Sinninghe Damsté J.S. (2016) The effect of improved
953 chromatography on GDGT based paleoproxies. Org. Geochem. 93, 1-6.
954 Huguet C., Hopmans E. C., Febo-Ayala W., Thompson D. H., Sinninghe Damsté J. S. and
955 Schouten S. (2006) An improved method to determine the absolute abundance of
956 glycerol dibiphytanyl glycerol tetraether lipids. Org. Geochem. 37, 1036-1041.
957 Lê S., Josse J. and Husson F. (2008) FactoMineR: An R package for multivariate analysis. J.
958 Stat. Softw. 25, 1-18.
959 Li J., Pancost R. D., Naafs B. D. A., Huan Y., Cheng Z. and Xie S. (2016) Distribution of
960 glycerol dialkyl glycerol tetraether (GDGT) lipids in a hypersaline lake system. Org.
961 Geochem. 99, 113–124.
962 Loomis S. E., Russell J. M. and Sinninghe Damsté J. S. (2011) Distributions of branched
963 GDGTs in soils and lake sediments from western Uganda: Implications for a
964 lacustrine paleothermometer. Org. Geochem. 42, 739–751.
965 Loomis S. E., Russell J. M., Ladd B., Street-Perrott F. A. and Sinninghe Damsté J. S. (2012)
966 Calibration and application of the branched GDGT temperature proxy on East African
967 lake sediments. Earth Planet. Sci. Lett. 357–358, 277–288.
968 Loomis S. E., Russell J. M., Eggermont H., Verschuren D. and Sinninghe Damsté J. S.
969 (2014a) Effects of temperature, pH, and nutrient concentration on branched GDGT
970 distributions in East African lakes: Implications for paleoenvironmental
971 reconstruction. Org. Geochem. 66, 25–37.
972 Loomis S. E., Russell J. M., Heureux A. M., D'Andrea W. J. and Sinninghe Damsté J. S.
973 (2014b) Seasonal variability of branched glycerol dialkyl glycerol tetraethers
974 (brGDGTs) in a temperate lake system. Geochim. Cosmochim. Acta 144, 173–187.
975 Loomis S.E., Russell J.M., Verschuren D., Morrill C., De Cort G., Sinninghe Damsté J.S.,
976 Olago D., Eggermont H., Street-Perrott F.A. and Kelly M.A. (2017) The tropical lapse
977 rate steepened during the Last Glacial Maximum. Sci. Adv. 3, e1600815.
978 Miller D. R., Habicht M. H., Keisling B. A., Castañeda I. S. and Bradley R. S. (2018) A 900-
979 year New England temperature reconstruction from *in situ* seasonally produced
980 branched glycerol dialkyl glycerol tetraethers (brGDGTs), Clim. Past. 14, 1653-1667.

Moernaut J., Verschuren D., Charlet F., Kristen I., Fagot M. and De Batist M. (2010) The seismic-stratigraphic record of lake level fluctuations in Lake Challa: hydrological stability and change in equatorial East Africa over the last 140 kyr. Earth Planet. Sci. Lett. 290, 214–223.

Naafs B. D. A., Inglis G. N., Zheng Y., Amesbury M. J., Biester H., Bindler R., Blewett J., Burrows M. A., Castillo Torres D. D., Chambers F. M., Cohen A. D., Evershed P. and Feakins S. J. (2017a) Introducing global peat-specific temperature and pH calibrations based upon brGDGT bacterial lipids. Geochim. Cosmochim. Acta 208, 285–301.

Naafs B. D. A., Gallego-Sala A. V., Inglis G. N. and Pancost R. D. (2017b) Refining the global branched glycerol dialkyl glycerol tetraether (brGDGT) soil temperature calibration. Org. Geochem. 106, 48-56.

Oppermann B. I., Michaelis W., Blumenberg M., Frerichs J., Schulz H. M., Schippers A., Beaubien S.E and Krüger M. (2010) Soil microbial community changes as a result of long-term exposure to a natural CO_2 vent. Geochim. Cosmochim. Acta 74, 2697-2716.

Pancost R. D., and Sinninghe Damsté J. S. (2003) Carbon isotopic compositions of prokaryotic lipids as tracers of carbon cycling in diverse settings. Chemical Geology 195, 29-58.

Parfenova V. V., Gladkikh A. S. and Belykh O. I. (2013) Comparative analysis of biodiversity in the planktonic and biofilm bacterial communities in Lake Baikal. Microbiology 82, 91–101.

Payne B. R. (1970) Water balance of Lake Chala and its relation to groundwater from tritium and stable isotope data. J. Hydrol. 11, 47-58.

Pearson E. J., Juggins S., Talbot H. M., Weckstrom J., Rosen P., Ryves D. B., Roberts S. J. and Schmidt R. (2011) A lacustrine GDGT-temperature calibration from the Scandinavian Arctic to Antarctic: Renewed potential for the application of GDGT paleothermometry in lakes. Geochim. Cosmochim. Acta 75, 6225–6238.

Peterse F., Kim J. H., Schouten S., Klitgaard Kristensen D., Koc N. and Sinninghe Damsté J. S. (2009) Constraints on the application of the MBT/CBT palaeothermometer at high latitude environments (Svalbard, Norway). Org. Geochem. 40, 692–699.

Peterse F., Hopmans E. C., Schouten S., Mets A., Rijpstra W. I. C. and Sinninghe Damsté J. S. (2011) Identification and distribution of intact polar branched tetraether lipids in peat and soil. Org. Geochem. 42, 1007–1015.

Peterse F., van der Meer M. T. J., Schouten S., Weijers J. W. H., Fierer N., Jackson R. B., Kim J. H. and Sinninghe Damsté J. S. (2012) Revised calibration of the MBT–CBT

paleotemperature proxy based on branched tetraether membrane lipids in surface soils. Geochim. Cosmochim. Acta 96, 215–229.

Powers L. A., Werne J. P., Vanderwoude A. J., Sinninghe Damsté J. S., Hopmans E. C. and Schouten S. (2010) Applicability and calibration of the TEX_{86} paleothermometer in lakes. Org. Geochem. 41, 404–413.

Preheim S. P., Olesen S. W., Spencer S. J., Materna A., Varadharajan C., Blackburn M., Friedman J., Rodríguez J., Hemond H. and Alm E. J. (2016) Surveys, simulation and single-cell assays relate function and phylogeny in a lake ecosystem. Nature Microbiol. 1, 16130.

Russell J. M., Hopmans E. C., Loomis S. E., Liang J. and Sinninghe Damsté J. S. (2018) Distributions of 5- and 6-methyl branched glycerol dialkyl glycerol tetraethers (brGDGTs) in East African lake sediment: Effects of temperature, pH, and new lacustrine paleotemperature calibrations. Org. Geochem. 117, 56–69.

Schoon P. L., de Kluijver A., Middelburg J. J., Downing J. A., Sinninghe Damsté J. S. and Schouten S. (2013) Influence of lake water pH and alkalinity on the distribution of core and intact polar branched glycerol dialkyl glycerol tetraethers (GDGTs) in lakes. Org. Geochem. 60, 72–82.

Schouten S., Rijpstra W. I. C., Durisch-Kaiser E., Schubert C. J. and Sinninghe Damsté J. S. (2012) Distribution of glycerol dialkyl glycerol tetraether lipids in the water column of Lake Tanganyika. Org. Geochem. 53, 34–37.

Schouten S., Hopmans E. C. and Sinninghe Damsté J. S. (2013) The organic geochemistry of glycerol dialkyl glycerol tetraether lipids: A review. Org. Geochem. 54, 19–61.

Sinninghe Damsté J. S. (2016) Spatial heterogeneity of sources of branched tetraethers in shelf systems: The geochemistry of tetraethers in the Berau River delta (Kalimantan, Indonesia). Geochim. Cosmochim. Acta 186, 13–31.

Sinninghe Damsté J. S., Ossebaar J., Abbas B., Schouten S. and Verschuren D. (2009) Fluxes and distribution of tetraether lipids in an equatorial African lake: constraints on the application of the TEX_{86} palaeothermometer and BIT index in lacustrine settings. Geochim. Cosmochim. Acta 73, 4232–4249.

Sinninghe Damsté J. S., Rijpstra W. I. C., Hopmans E. C., Weijers J. W. H., Foesel B. U., Overmann J. and Dedysh S. N. (2011a) 13,16-Dimethyl octacosanedioic acid (iso-diabolic acid): A common membrane-spanning lipid of Acidobacteria subdivisions 1 and 3. Appl. Environ. Microbiol. 77, 4147–4154.

1048 Sinninghe Damsté J.S., Verschuren D., Ossebaar J., Blokker J., van Houten R., van der Meer
1049 M.T.J., Plessen B. and Schouten S. (2011b) A 25,000-year record of climate-induced
1050 changes in lowland vegetation of eastern equatorial Africa revealed by the stable
1051 carbon-isotopic composition of fossil plant leaf waxes. Earth Planet. Sci. Lett 302,
1052 236-246.
1053 Sinninghe Damsté J.S., Rijpstra W.I.C., Hopmans E.C., Foesel B., Wüst P., Overmann J.,
1054 Tank M., Bryant D., Dunfield P., Houghton K. and Stott M. (2014) Ether- and ester-
1055 bound iso-diabolic acid and other lipids in Acidobacteria of subdivision 4. Appl.
1056 Environ. Microbiol. 80, 5207-5218.
1057 Sinninghe Damsté J. S., Rijpstra W. I. C., Foesel B. U., Huber K., Overmann J., Nakagawa S.,
1058 Kim J. J., Dunfield P., Dedysh S. and Villanueva L. (2018) An overview of the
1059 occurrence of ether- and ester-linked iso diabolic acid membrane lipids in microbial
1060 cultures of the Acidobacteria: Implications for brGDGT paleoproxies for temperature
1061 and pH. Org. Geochem. 124, 63-76.
1062 Sun Q., Chu G., Liu M., Xie M., Li S., Ling Y., Wang X., Shi L., Jia G. and Lu H. (2011)
1063 Distributions and temperature dependence of branched glycerol dialkyl glycerol
1064 tetraethers in recent lacustrine sediments from China and Nepal. J. Geophys. Res. 116,
1065 G01008.
1066 Tierney J. E. and Russell J. M. (2009) Distributions of branched GDGTs in a tropical lake
1067 system: implications for lacustrine application of the MBT/CBT paleoproxy. Org.
1068 Geochem. 40, 1032–1036.
1069 Tierney J. E., Russell J. M., Huang Y., Sinninghe Damsté J. S., Hopmans E. C. and Cohen A.
1070 S. (2008) Northern hemisphere controls on tropical southeast African climate during
1071 the past 60,000 years. Science 322, 252–255.
1072 Tierney J. E., Russell J. M., Eggermont H., Hopmans E. C., Verschuren D. and Sinninghe
1073 Damsté J. S. (2010) Environmental controls on branched tetraether lipid distributions
1074 in tropical East African lake sediments. Geochim. Cosmochim. Acta 74, 4902–4918.
1075 Tierney J. E., Schouten S., Pitcher A., Hopmans E. C. and Sinninghe Damsté J. S. (2012)
1076 Core and intact polar glycerol dialkyl glycerol tetraethers (GDGTs) in Sand Pond,
1077 Warwick, Rhode Island (USA): insights into the origin of lacustrine GDGTs.
1078 Geochim. Cosmochim. Acta 77, 561–581.
1079 van Bree L. G. J., Rijpstra W. I. C., Al-Dhabi N. A., Verschuren D., Sinninghe Damsté J. S.
1080 and de Leeuw J. W. (2016) *Des*-A-lupane in an East African lake sedimentary record

as a new proxy for the stable carbon isotopic composition of C_3 plants. Org. Geochem. 101, 132-139.

van Bree L. G. J., Peterse F., van der Meer M. T. J., Middelburg J. J., Negash A. M. D., De Crop W., Cocquyt C., Wieringa J. J., Verschuren D. and Sinninghe Damsté J. S. (2018) Seasonal variability in the abundance and stable carbon-isotopic composition of lipid biomarkers in suspended particulate matter from a stratified equatorial lake (Lake Chala, Kenya/Tanzania): Implications for the sedimentary record. Quat. Sci. Rev. 192, 208-224.

Verschuren D., Sinninghe Damsté J. S., Moernaut J., Kristen I., Blaauw M., Fagot M., Haug G. H. and CHALLACEA Project Members (2009) Half-precessional dynamics of monsoon rainfall near the East African Equator. Nature 462, 637-641.

Volkman J. K., Barrett S. M., Blackburn S. I., Mansour M. P., Sikes E. L. and Gelin F. (1998) Microalgal biomarkers: A review of recent research developments. Org. Geochem. 29, 1163-1179.

Wang H. Y., Liu W. G., Zhang C. L. L., Wang Z., Wang J. X., Liu Z. H. and Dong H. L. (2012) Distribution of glycerol dialkyl glycerol tetraethers in surface sediments of Lake Qinghai and surrounding soil. Org. Geochem. 47, 78–87.

Weber Y., De Jonge C., Rijpstra W. I. C., Hopmans E. C., Stadnitskaia A., Schubert C. J., Lehmann M. F., Sinninghe Damsté J. S. and Niemann H. (2015) Identification and carbon isotope composition of a novel GDGT isomer in lake sediments: Evidence for lacustrine brGDGT production? Geochim. Cosmochim. Acta 154, 118–129.

Weber Y., Sinninghe Damsté J. S., Zopfi J., De Jonge C., Gili A., Schubert C. J., Lepori F., Lehmann M. F. and Niemann H. (2018) Redox-dependent niche differentiation provides evidence for multiple bacterial sources of glycerol tetraether lipids in lakes. Proc. Natl. Acad. Sci. U.S.A. 115, 10926-10931.

Weijers J. W. H., Schouten S., Hopmans E. C., Geenevasen J. A. J., David O. R. P., Coleman J. M., Pancost R. D. and Sinninghe Damsté J. S. (2006) Membrane lipids of mesophilic anaerobic bacteria thriving in peats have typical archaeal traits. Environ. Microbiol. 8, 648–657.

Weijers J. W. H., Schefuß E., Schouten S. and Sinninghe Damsté J. S. (2007a) Coupled thermal and hydrological evolution of tropical Africa over the last deglaciation. Science 315, 1701–1704.

1113 Weijers J. W. H., Schouten S., van den Donker J. C., Hopmans E. C. and Sinninghe Damsté J.
1114 S. (2007b) Environmental controls on bacterial tetraether membrane lipid distribution
1115 in soils. Geochim. Cosmochim. Acta 71, 703–713.
1116 Weijers J. W. H., Panoto E., van Bleijswijk J., Schouten S., Rijpstra W. I. C., Balk M., Stams
1117 A. J. M. and Sinninghe Damsté J. S. (2009) Constraints on the biological source(s) of
1118 the orphan branched tetraether membrane lipids. Geomicrobiol. J. 26, 402–414.
1119 Weijers J. W. H., Wisenberg G. L. B., Bol R., Hopmans E. C. and Pancost R. D. (2010)
1120 Carbon isotopic composition of branched tetraether membrane lipids in soils suggest a
1121 rapid turnover and a heterotrophic life style of their source organism(s).
1122 Biogeosciences 7, 2959–2973.
1123 Weijers J. W. H., Bernhardt B., Peterse F., Werne J. P., Dungait J. A. J., Schouten S. and
1124 Sinninghe Damsté J. S. (2011) Absence of seasonal patterns in MBT–CBT mid-
1125 latitude soils. Geochim. Cosmochim. Acta 75, 3179–3190.
1126 White, D.C., Davis, W.M., Nickels, J.S., King, J.D., and Bobbie, R.J. (1979). Determination
1127 of the sedimentary microbial biomass by extractible lipid phosphate. Oecologia 40,
1128 51-62.
1129 Wolff C., Haug G. H., Timmermann A., Sinninghe Damsté J. S., Brauer A., Sigman D. M.,
1130 Cane M. A. and Verschuren, D. (2011) Reduced interannual rainfall variability in East
1131 Africa during the Last Ice Age. Science 333, 743-747.
1132 Wolff C., Kristen-Jenny I., Schettler G., Plessen B., Meyer H., Dulski P., Naumann R., Brauer
1133 A., Verschuren D. and Haug G. H. (2014) Modern seasonality in Lake Challa
1134 (Kenya/Tanzania) and its sedimentary documentation in recent lake sediments.
1135 Limnol. Oceanogr. 59, 1621-1636.
1136 Woltering M., Werne J. P., Kish J. L., Hicks R., Sinninghe Damsté J. S. and Schouten S.
1137 (2012) Vertical and temporal variability in concentration and distribution of
1138 thaumarchaeotal tetraether lipids in Lake Superior and the implications for the
1139 application of the TEX_{86} temperature proxy. Geochim. Cosmochim. Acta 87, 136-153.
1140 Zhang J., Kobert K., Flouri T. and Stamatakis A. (2013) PEAR: A fast and accurate Illumina
1141 Paired-End reAd mergeR. Bioinformatics 30, 614-620.
1142 Zheng Y., Pancost R. D., Liu X., Wang Z., Naafs B. D. A., Xie X., Liu Z., Yu X. and Yang H.
1143 (2017) Atmospheric connections with the North Atlantic enhanced the deglacial
1144 warming in northeast China. Geology 45, 1031-1034.

1145 Zimmermann J, Portillo M. C., Serrano L., Ludwig W. and Gonzalez J. M. (2012)
1146 Acidobacteria in freshwater ponds at Doñana National Park, Spain. Microb. Ecol. 63,
1147 844–55.
1148 Zink K. G., Leythaeuser D., Melkonian M. and Schwark L. (2001) Temperature dependency
1149 of long-chain alkenone distributions in recent to fossil limnic sediments and lake
1150 waters. Geochim. Cosmochim. Acta 65, 253–265.
1151

Figure captions

Figure 1. Molecular structures of brGDGTs, consisting of two ether-linked dialkyl chains with zero to two additional methyl branches (I, II and III) and zero to two cyclopentyl moieties (suffixes a, b and c). The 6-methyl isomers are denoted with a prime. Compounds indicated in bold are the eight most common brGDGTs encountered in Lake Chala, and focused upon in data presentation and discussion.

Figure 2. A: Location of Lake Chala in East Africa, on the border of Kenya and Tanzania, and B: The bathymetry of Lake Chala situated within its steep-sided crater catchment (outer bold full line), with sampling locations of suspended particulate matter (SPM; black square), settling particles (sediment trap; open triangle), surficial lake-bottom sediments (grey triangles), and terrestrial soils (open circles). Bathymetry adapted from Moernaut et al. (2010).

Figure 3. Temperature (ºC) variation within the water column of Lake Chala between September 2010 and January 2015, based on automatic loggers suspended at 2, 10, 20, 25, 50 and 80 m depth (as available), in relation to the Bodé et al. (2020) time series of mean monthly air temperature (MMAT; stippled line) at a savanna site ~25 km west of Lake Chala. The dark blue line shows the position of the oxycline between September 2013 and December 2015, based on the shallowest depth with dissolved oxygen concentration <0.2 mg L^{-1} as measured by monthly water-column profiling (van Bree et al., 2018). Grey shading highlights the seasonal periods of upper water-column stratification (S) and deep mixing (DM). Due to the hiatus in temperature logging data, timing of the start and end of the deep-mixing period in 2012 was inferred from the MMAT trend.

Figure 4. Depth-interpolated concentrations (in ng L^{-1}) of the summed and eight most common individual brGDGT compounds in SPM collected at eight depth intervals (occasionally 13) between 0 and 80 m in Lake Chala, at approximately monthly intervals between September 2013 and January 2015. Also indicated is the varying position of the oxycline (bold stippled line) in relation to the static position of the sediment trap at 35

m depth (thin dashed line), which separates the $SPM_{abovetrap}$ and $SPM_{belowtrap}$ zones. Grey background shading indicates the seasonal periods of upper water-column stratification (S) and deep mixing (DM), as in Fig.3.

Figure 5. Average distribution of brGDGTs in the various sets of samples analyzed in this study. A: Temporally-integrated, concentration- or flux-weighted average fractional abundances of individual brGDGT compounds in SPM from above (light blue) and below (dark blue) the sediment trap, and settling particles trapped over the 17-month period of SPM sampling (Sept-2013 to Jan-2015; light green) and over the longer 53-month period starting three years earlier (Sept-2010 to Jan-2015, dark green), compared with average fractional abundances of the same brGDGTs in surficial lake-bottom sediments (orange) and catchment soils (red). B: Proportion of tetra-, penta- and hexamethyl brGDGTs in SPM from above (light blue circles) and below (dark blue circles) the sediment trap, and in settling particles (green squares), lake sediments (orange diamonds) and soils (red triangles) plotted over corresponding data from the surficial bottom sediments of 65 East African Lakes (grey triangles; Russell et al., 2018).

Figure 6. Principal component analysis (PCA) of the fractional abundances of the eight major brGDGTs in SPM (n = 143) and settling particles (n = 53) from Lake Chala. A-B: PC1 vs PC2 (A) and PC2 vs PC3 (B) of the SPM samples, with black vectors indicating the PCA scores of individual brGDGTs, and blue vectors showing the PCA scores of environmental variables added passively. Temperature and pH are measured (0-50 m depth, van Bree et al., 2018) and assumed constant from 50 m to 80 m depth. C-D: PC1 vs PC2 (C) and PC2 vs PC3 (D) of the settling particles, with black vectors indicating the PCA scores of individual brGDGTs, and blue vector showing the PCA score of the total bulk settling flux added passively. E: Combined PCA of the fractional abundances of the (mainly aquatic) brGDGTs in all SPM (blue circles) and settling-particle (green squares) samples, with distinction between SPM from above (light blue) and below (dark blue) the sediment trap. The PCA scores of lake sediments (orange diamonds) and soils (red triangles) were added passively.

Figure 7. Time series of settling-particle data from Lake Chala, based on 53 months of sediment-trap deployment between August 2010 and January 2015. A: Temporal variation in total bulk dry flux (mg m^{-2} day^{-1}). B: Total brGDGT flux (ng m^{-2} day^{-1}) with indication of the proportions

of tetra-methylated (green), 5-methyl (purple) and 6-methyl (brown) brGDGTs. C: Fraction of 6-methyl penta- and hexamethylated brGDGTs (IR_{6ME}). D-F: Fractional abundances of brGDGTs Ib+IIb (D), IIa′+IIIa′ (E) and Ia (F). G: Reconstructed mean annual air temperature (MAAT), using the EAL calibration of Russell et al. (2018). Also indicated are MMAT (red dashed line) and MAAT (black dashed line), both from Bodé et al. (2020). H: Reconstructed surface-water pH, using the EAL calibration of Russell et al. (2018), and pH measured at the surface (0 m) during the period September 2013 to January 2015 (van Bree et al., 2018). The right-hand panels show boxplots indicating median, interquartile, minimum, maximum and outlier values of the bulk and brGDGT fluxes and proxies (A-B), suspended-particulate data (SPM in C-H; n = 143), settling-particle data (ST in C-H; n = 53), lake-sediment data (SED in C-H; n = 3) and catchment soil data (SOIL in C-H; n = 7). These box plots are superimposed with flux- or abundance-weighted average values of the same for $SPM_{abovetrap}$ (light blue circle), $SPM_{belowtrap}$ (dark blue circle), settling particles trapped over the 17-month period of SPM sampling (September 2013 to January 2015, crossed green square) or over the 53-month period starting three years earlier (September 2010 to January 2015, green square), lake sediments (orange diamond) and soils (red triangle). Grey background shading highlights the seasonal periods of upper water-column stratification (S) and deep mixing (DM).

Figure 8. Correlation matrix (R^2; represented by shades of blue) between the absolute concentration of the eight major brGDGTs in Lake Chala SPM (ng L^{-1}) and estimated 16S rRNA gene abundances (copies L^{-1}, see details in text). A: Acidobacteria SD 6, 18, 19 and 21, and the sum of all Acidobacteria. The Acidobacterial SD OTUs are present in at least 10% of the SPM samples measured for both brGDGTs and gene abundances. Only SDs that correlate with at least one brGDGT with an $R^2 \geq 0.05$ are shown. B: The 14 taxa of bacteria displaying highest correlation with individual brGDGTs, divided in clusters of highest correlation with Ib and IIb or with the other brGDGTs. The bacterial OTUs are present in at least 10% of the SPM samples measured for both biomarkers and gene abundances. Only SDs that correlate with at least one brGDGTs with $R^2 \geq$ 0.2 are shown.

Supplement and data availability

All data are available in the supplementary tables at PANGAEA:

https://doi.pangaea.de/10.1594/PANGAEA.922776 (Tables S.1 and S.5)

https://doi.pangaea.de/10.1594/PANGAEA.922780 (Table S.2)

https://doi.pangaea.de/10.1594/PANGAEA.922781 (Table S.3)

https://doi.pangaea.de/10.1594/PANGAEA.922783 (Table S.4)

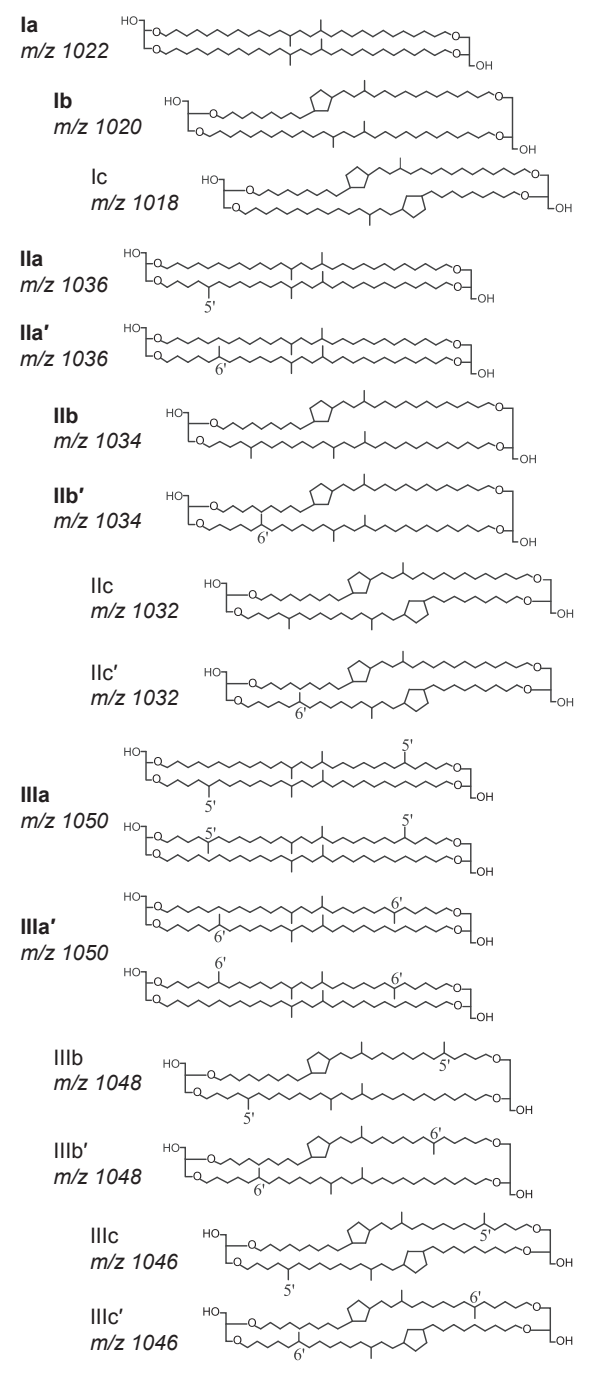
Ia
m/z 1022
Ib
m/z 1020
Ic
m/z 1018
IIa
m/z 1036
IIa'
m/z 1036
IIb
m/z 1034
IIb'
m/z 1034
IIc
m/z 1032
IIc'
m/z 1032
IIIa
m/z 1050
IIIa'
m/z 1050
IIIb
m/z 1048
IIIb'
m/z 1048
IIIc
m/z 1046
IIIc'
m/z 1046
HO
OH
5'
6'

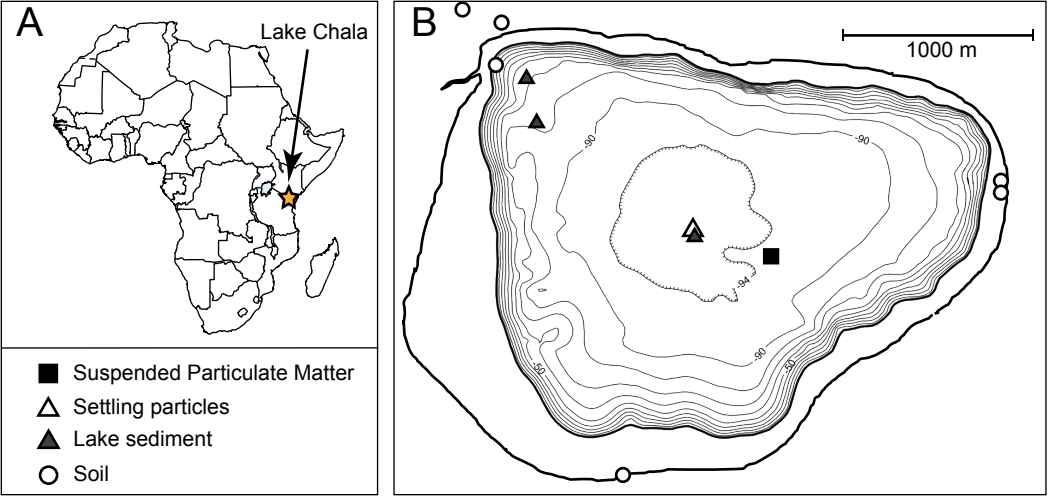
A
Lake Chala
B
1000 m
-90
-94
-92
-96
Suspended Particulate Matter
Settling particles
Lake sediment
Soil

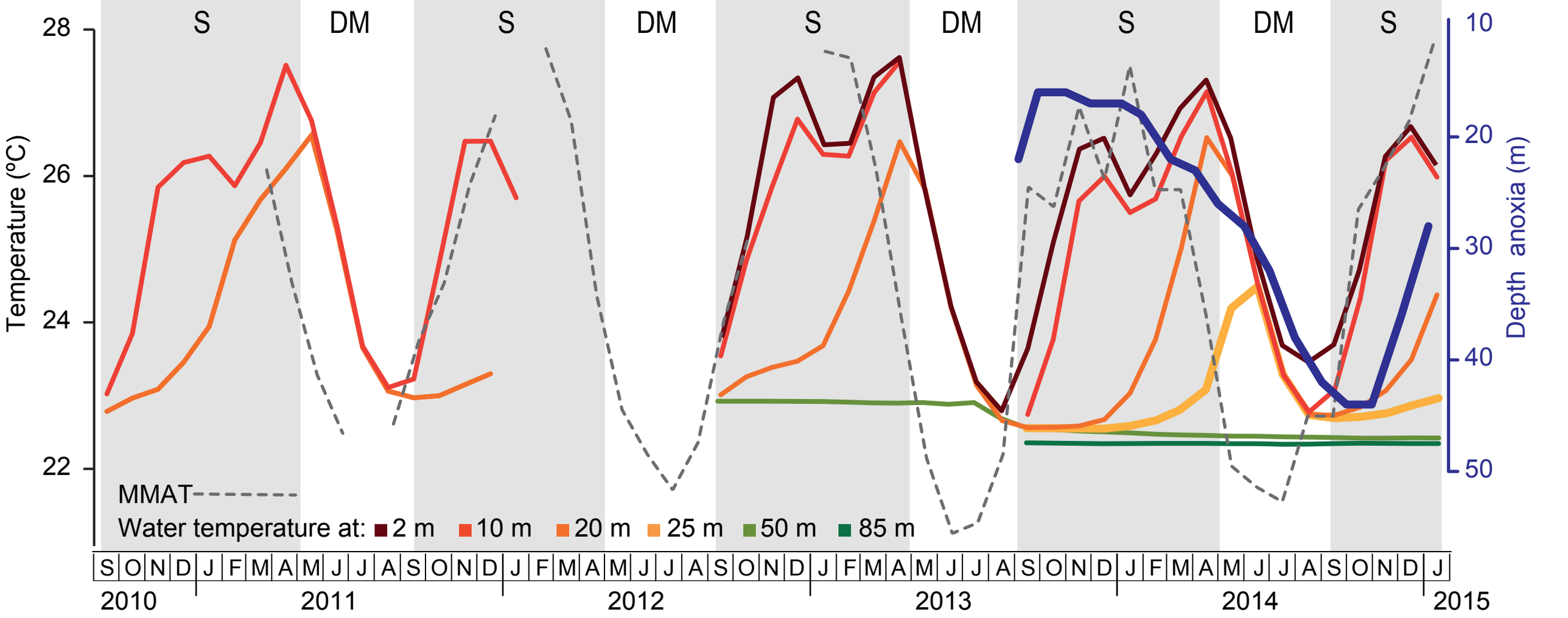
S
DM
S
DM
S
DM
S
DM
S
28
26
24
22
Temperature (°C)
10
20
30
40
50
Depth anoxia (m)
MMAT
Water temperature at: 2 m 10 m 20 m 25 m 50 m 85 m
S O N D J F M A M J J A S O N D J F M A M J J A S O N D J F M A M J J A S O N D J F M A M J J A S O N D J
2010
2011
2012
2013
2014
2015

S DM S

Ia

Ib

IIa

oxic

anoxic

IIb

IIIa

IIa′

IIb′

IIIa′

ΣbrGDGTs

Depth (m)

0 10 20 30 40 50 60 70 80

S O N D J F M A M J J A S O N D J

2013 2014 2015

ng L^{-1}

0.0 - 0.25
0.25 - 0.5
0.5 - 0.75
0.75 - 1.0
1.0 - 1.25
1.25 - 1.50
1.50 - 2.0
2.0 - 3.0
3.0 - 4.0
4.0 - 5.0
5.0 - 6.0
6.0 - 7.0
7.0 - 8.0
8.0 - 12.0
12.0 - 16.0
16.0 - 25.0

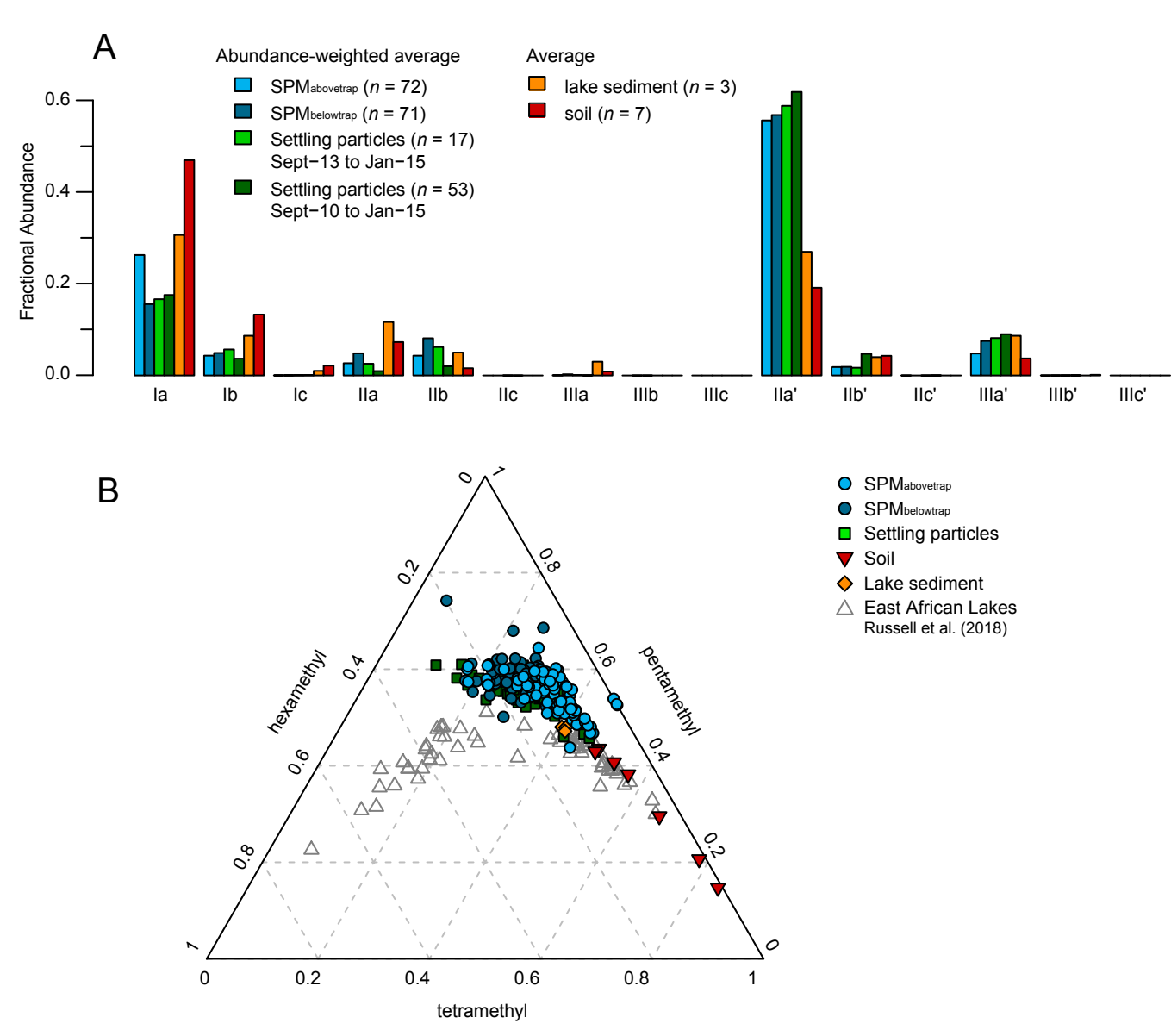
A
Abundance-weighted average
SPMabovetrap (n = 72)
SPMbelowtrap (n = 71)
Settling particles (n = 17) Sept−13 to Jan−15
Settling particles (n = 53) Sept−10 to Jan−15
Average
lake sediment (n = 3)
soil (n = 7)
Fractional Abundance
0.0
0.2
0.4
0.6
Ia
Ib
Ic
IIa
IIb
IIc
IIIa
IIIb
IIIc
IIa'
IIb'
IIc'
IIIa'
IIIb'
IIIc'
B
SPMabovetrap
SPMbelowtrap
Settling particles
Soil
Lake sediment
East African Lakes
Russell et al. (2018)
hexamethyl
pentamethyl
tetramethyl
0
0.2
0.4
0.6
0.8
1

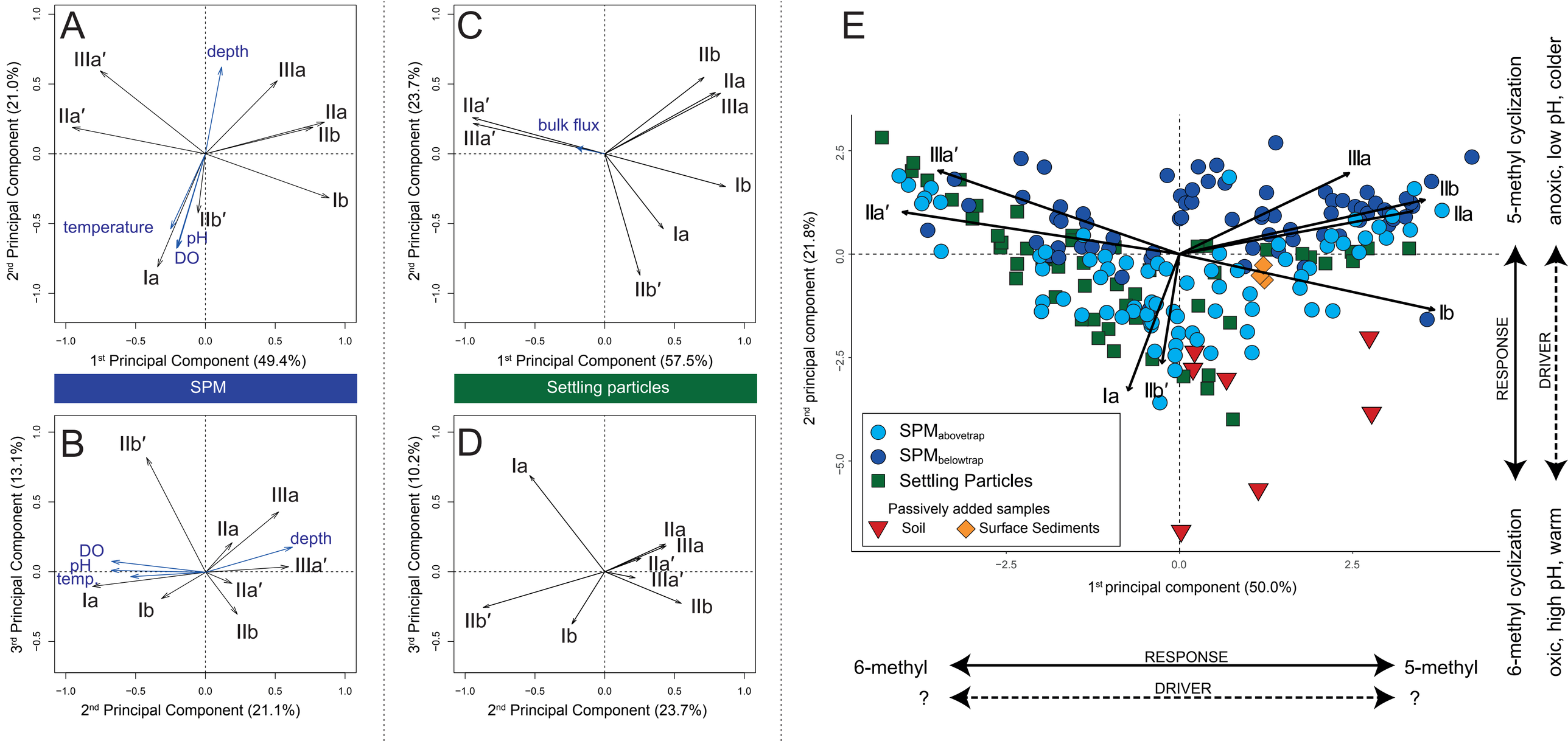
A
IIIa′
depth
IIIa
IIa′
IIa
IIb
Ib
temperature
IIb′
pH
DO
Ia
2nd Principal Component (21.0%)
1st Principal Component (49.4%)
SPM
C
IIb
IIa
IIIa
IIa′
bulk flux
IIIa′
Ib
Ia
IIb′
2nd Principal Component (23.7%)
1st Principal Component (57.5%)
Settling particles
B
IIb′
IIIa
IIa
depth
DO
pH
temp
IIIa′
Ia
Ib
IIa′
IIb
3rd Principal Component (13.1%)
2nd Principal Component (21.1%)
D
Ia
IIa
IIIa
IIa′
IIIa′
IIb
IIb′
Ib
3rd Principal Component (10.2%)
2nd Principal Component (23.7%)
E
IIIa′
IIIa
IIa′
IIb
IIa
Ib
Ia
IIb′
SPMabovetrap
SPMbelowtrap
Settling Particles
Passively added samples
Soil
Surface Sediments
2nd principal component (21.8%)
1st principal component (50.0%)
5-methyl cyclization
anoxic, low pH, colder
RESPONSE
DRIVER
6-methyl cyclization
oxic, high pH, warm
6-methyl
RESPONSE
5-methyl
?
DRIVER
?

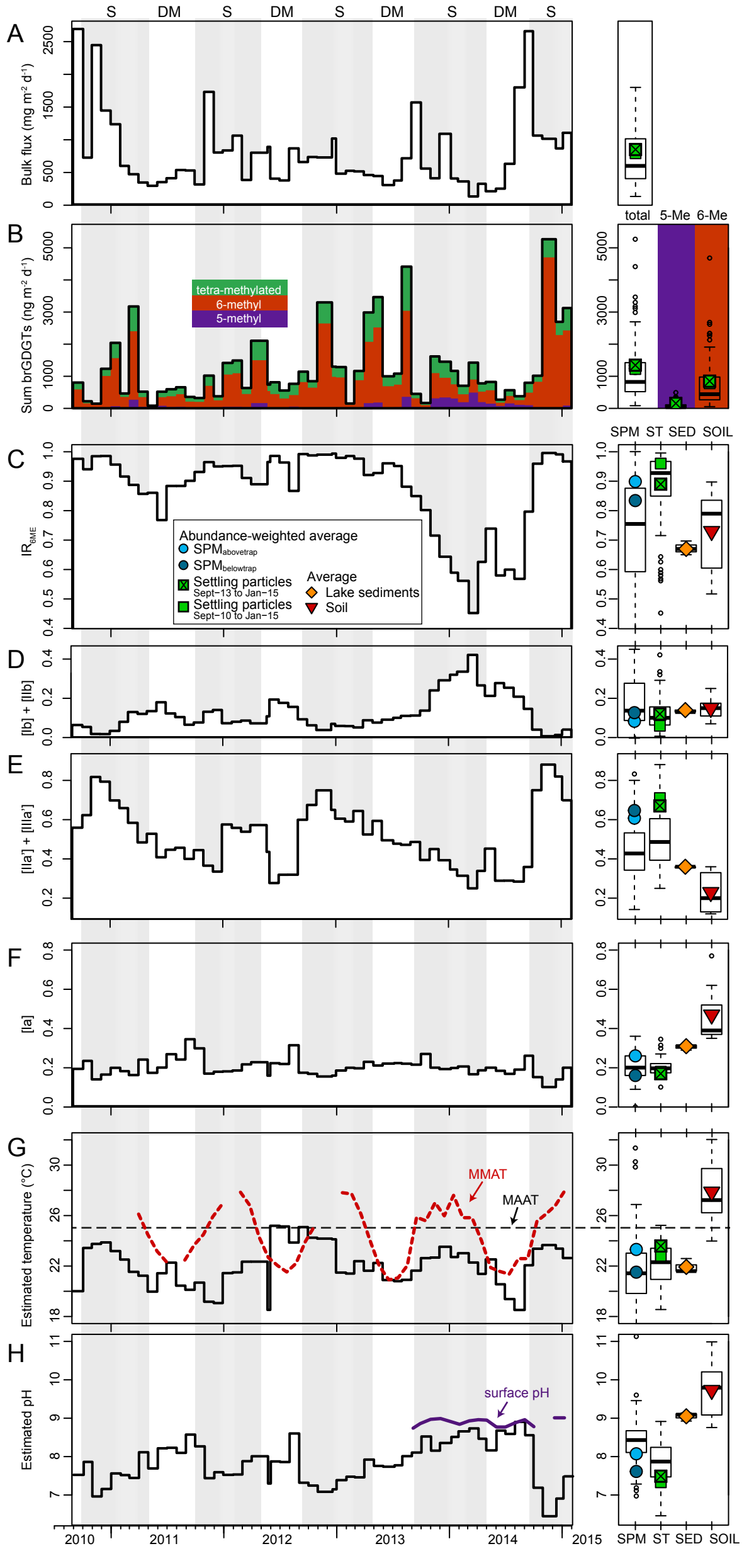
S
DM
A
Bulk flux (mg m-2 d-1)
B
Sum brGDGTs (ng m-2 d-1)
tetra-methylated
6-methyl
5-methyl
total
5-Me
6-Me
C
IR6ME
Abundance-weighted average
SPMabovetrap
SPMbelowtrap
Settling particles Sept−13 to Jan−15
Settling particles Sept−10 to Jan−15
Average
Lake sediments
Soil
SPM
ST
SED
SOIL
D
[Ib] + [IIb]
E
[IIa'] + [IIIa']
F
[Ia]
G
Estimated temperature (°C)
MMAT
MAAT
H
Estimated pH
surface pH
2010
2011
2012
2013
2014
2015

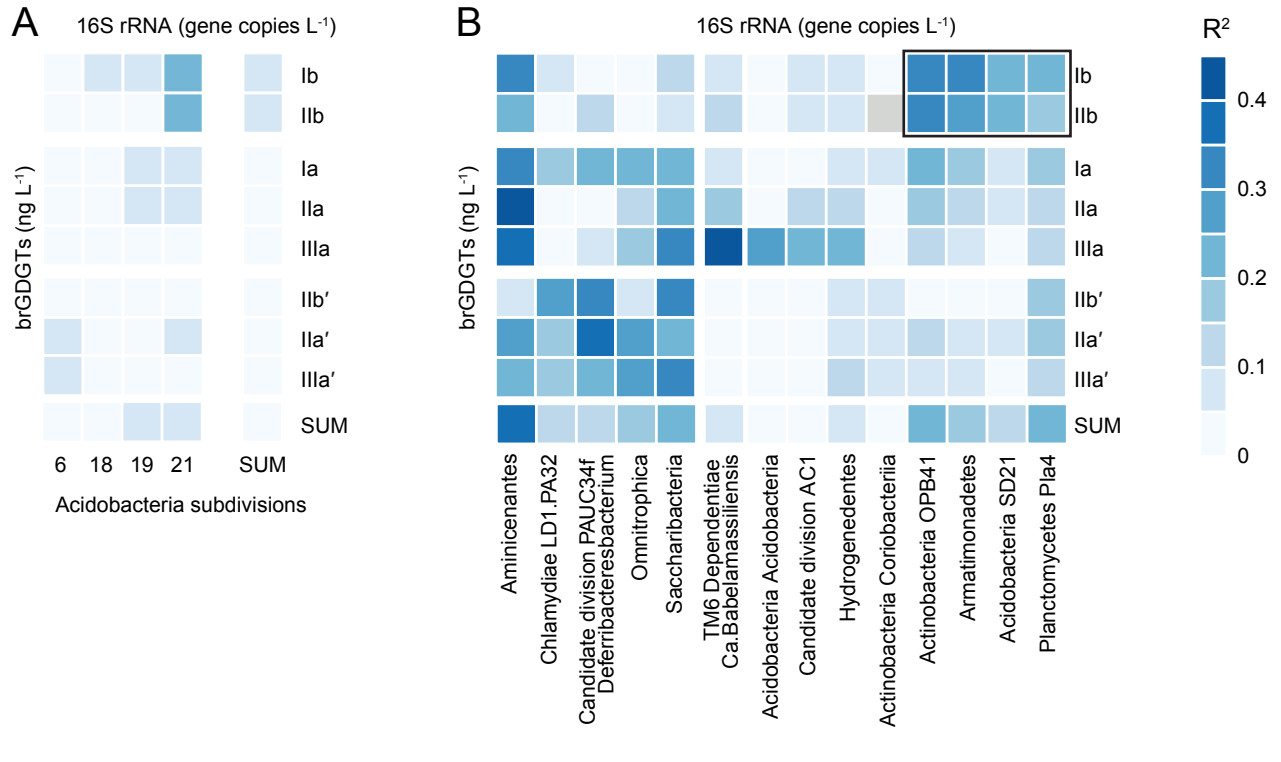
A
16S rRNA (gene copies L-1)
Ib
IIb
Ia
IIa
IIIa
IIb′
IIa′
IIIa′
SUM
brGDGTs (ng L-1)
6
18
19
21
SUM
Acidobacteria subdivisions
B
16S rRNA (gene copies L-1)
brGDGTs (ng L-1)
Aminicenantes
Chlamydiae LD1.PA32
Candidate division PAUC34f Deferribacteresbacterium
Omnitrophica
Saccharibacteria
TM6 Dependentiae Ca.Babelamassiliensis
Acidobacteria Acidobacteria
Candidate division AC1
Hydrogenedentes
Actinobacteria Coriobacteriia
Actinobacteria OPB41
Armatimonadetes
Acidobacteria SD21
Planctomycetes Pla4
R2
0.4
0.3
0.2
0.1
0